A Positive Feedback Regulation of SnRK1 Signaling by Autophagy in Plants

Chao Yang^{1,2}, Xibao Li¹, Shunquan Chen¹, Lianming Yang¹, Jun Liao¹, Kailin Li¹, Jun Zhou¹, Wenjin Shen¹, Xiaohong Zhuang³, Diane C. Bassham⁴ and Caiji Gao^{1, *}

¹Guangdong Provincial Key Laboratory of Biotechnology for Plant Development, School of Life Sciences, South China Normal University, Guangzhou, 510631, China ²Guangdong Provincial Key Laboratory of Applied Botany & Agriculture and Biotechnology Research Center, South China Botanical Garden, Chinese Academy of Sciences, Guangzhou, 510650, China

³School of Life Sciences, Centre for Cell and Developmental Biology, The Chinese University of Hong Kong, Shatin, New Territories, Hong Kong, China

⁴Department of Genetics, Development and Cell Biology, Iowa State University, Ames, IA, USA.

*Address correspondence to Caiji Gao (gaocaiji@m.scnu.edu.cn).

ABSTRACT

SnRK1, an evolutionarily conserved heterotrimeric kinase complex acting as a key metabolic sensor to maintain energy homeostasis in plants, is an upstream activator of autophagy, an important cellular degradation pathway essential for healthy growth of plants. But whether and how autophagy pathway involves in the feedback regulation of SnRK1 activity remains unknown. Here, we identified a clade of plant-specific FCS-like zinc finger (FLZ) proteins as up-to-now unknown ATG8-interacing partners, which actively inhibit the SnRK1 signaling by repressing the T-loop phosphorylation of the catalytic α subunits of SnRK1, thereby negatively modulating autophagy and plant tolerance to energy deprivation caused by long-term carbon starvation. Interestingly, these AtFLZs are transcriptionally repressed by low energy stress and AtFLZs proteins undergo an autophagy-dependent pathway to be delivered to vacuole for degradation, thereby relieving their repression on SnRK1 signaling. Bioinformatic analysis showed that the ATG8-FLZ-SnRK1 regulatory axis is originated in gymnosperms and seems to be highly conserved during the evolution of seed plants. Coinciding with this, knockout of the ATG8-interacted ZmFLZ14 confers enhanced tolerance to dark treatment in maize. Our findings thus reveal a previously unknown mechanism by which selective autophagy contributes to the positive feedback regulation of SnRK1 signaling, thereby conferring better adaptation of plants to stressful environments.

Key words: SnRK1, autophagy, ATG8, FLZ, carbon starvation

INTRODUCTION

Energy homeostasis is vital to all living organisms. As sessile and autotrophic organisms, plants are frequently encountered a diverse array of environmental stresses such as drought, dark and nutrient deficiency that usually result in cellular energy deficit (Tome et al., 2014). Thus, controlling energy homeostasis is a major challenge for plants during their adaptation to unfavorable growth conditions. The SNF1-related protein kinase 1 (SnRK1) is a plant ortholog of yeast sucrose non-fermentable 1 (SNF1) and mammalian AMP-dependent protein kinase (AMPK), which acts as a metabolic sensor and plays essential roles in maintaining cellular energy homeostasis for plant healthy growth and survival (Emanuelle et al., 2015; Williams et al., 2014). The activity of SnRK1 is strictly controlled, as either over activation or false repression is detrimental for plant growth (Baena-Gonzalez et al., 2007; Chen et al., 2017). SnRK1 can be activated by energy starvation as a result of prolonged darkness, hypoxia, or chemical inhibition of photosynthesis, while can be inhibited by exogenous sucrose or glucose (Ananieva et al., 2008; Baena-Gonzalez et al., 2007; Coello and Martinez-Barajas, 2014).

SnRK1 is a heterotrimeric complex with a catalytic (α) and two regulatory (β, and plant-specific βy) subunits (Broeckx et al., 2016; Emanuelle et al., 2015; Margalha et al., 2016). The catalytic α subunit contributes to the kinase activity of this complex, and the regulatory subunits are required for modulating the stability, substrate specificity, subcellular localization or kinase activity of SnRK1 complex (Broeckx et al., 2016; Margalha et al., 2016). Arabidopsis thaliana encodes three isoforms of the catalytic α subunit, namely SnRK1.1 (KIN10/AKIN10), SnRK1.2 (KIN11/AKIN11) and SnRK1.3 (KIN12/AKIN12) (Emanuelle et al., 2015; Fragoso et al., 2009; Williams et al., 2014), but only SnRK1.1 and SnRK1.2 appear to be expressed (Fragoso et al., 2009) and SnRK1.1 is responsible for most of the SnRK1 activity (Jossier et al., 2009). SnRK1.1 is composed of a N-terminal kinase domain harboring the conserved T-loop, and a C-terminal regulatory domain, which encompasses a ubiquitin-associated (UBA) domain and a kinase-associated 1 (KA1) domain (Emanuelle et al., 2015; Williams et al., 2014). SnRK1 activity is positively regulated by upstream kinases including SnRK1-activating kinase-1 and -2 (SnAK1 and SnAK2), which are responsible for phosphorylating the conserved T-loop threonine in SnRK1 α subunits (Glab et al., 2017; Shen et al., 2009). On the other hand, two type 2C protein phosphatases, ABA-INSENSITIVE 1 (ABI1) and PP2CA, can interact with and dephosphorylate SnRK1 α subunits, thereby negatively regulating SnRK1 activity (Rodrigues et al., 2013). The activity of SnRK1 is also tightly monitored by the availability of sugars and sugar-phosphates. For an example, trehalose 6-phosphate (T6P) can directly bind to SnRK1.1 and weaken SnAK-SnRK1.1 association, thereby reducing both of phosphorylation level and kinase activity of SnRK1.1 (Zhai et al., 2018).

In addition, SnRK1 is modulated by SUMO E3 ligase SIZ1-mediated SUMOylation, followed by ubiquitination and 26S proteasomal degradation of SnRK1.1 (Crozet et al., 2016).

SnRK1 serves as a central metabolic regulator of cellular energy homeostasis by activating catabolic reactions and inhibiting energy-consuming anabolic processes (Baena-Gonzalez et al., 2007; Robertlee et al., 2017). As a classic example, SnRK1 can activate cell autophagy, an evolutionarily conserved self-digestion process essential for the maintenance of cellular homoeostasis (Marshall and Vierstra, 2018). SnRK1-mediated autophagy regulation occurs both at transcriptional and post-translational levels in plants (Baena-Gonzalez et al., 2007; Chen et al., 2017; Huang et al., 2019; Soto-Burgos and Bassham, 2017). At the transcriptional level, SnRK1 is involved in promoting the expression of several important autophagy-related (ATG) genes, including ATG2, ATG5, ATG8e and ATG18a, in response to energy starvation (Baena-Gonzalez et al., 2007; Chen et al., 2017). At the post-translational level, upon short-term carbon starvation treatment, SnRK1 prominently phosphorylates ATG1 to initiate autophagy (Chen et al., 2017), while under long-term carbon starvation conditions, SnRK1 can phosphorylate ATG6 to activate autophagy via an ATG1-independent pathway (Huang et al., 2019). Consistently, the activation of autophagy by various abiotic stresses (e.g., salt, osmotic, oxidative, endoplasmic reticulum stresses and fixed-carbon or nitrogen deficiency) is compromised in the loss-of-function snrk1.1 mutant, but is enhanced in the SnRK1.1 overexpression plants (Chen et al., 2017; Soto-Burgos and Bassham, 2017). Interestingly, blocking autophagy by depletion of ATG5 or ATG7 can completely abolish the increased tolerance of SnRK1.1-overexpressing plants to nutrient starvation, suggesting that the action of SnRK1 in enhancing plant stress tolerance largely depends on a functional autophagy pathway (Chen et al., 2017). These findings highlight the positive roles of SnRK1 on autophagy activation in plants, but whether, and if so how, autophagy pathway involves in the regulation of SnRK1 activity remains totally unknown.

In this study, we identified seven plant-specific FCS-like zinc finger (FLZ) proteins as up-to-now unknown ATG8-interacting partners, which acts repressors of SnRK1 signaling to negatively modulates autophagy and plant tolerance to carbon starvation. On the other hand, under long term carbon starvation, FLZs proteins undergo an autophagy-dependent pathway to be delivered to vacuole for degradation, thereby constituting positive feedback regulation to relieve their repression on SnRK1 signaling. We also found that this ATG8-FLZ-SnRK1 regulatory axis is highly conserved in seed plants. Thus, our work reveals an evolutionarily conserved mechanism that precisely control the cellular energy homeostasis by orchestrating SnRK1 signaling and autophagy pathway, thereby conferring plant better tolerance and survival under stressful conditions.

RESULTS

Identification of the AIM-containing FLZ proteins as interactors of ATG8 in Arabidopsis

To explore the molecular mechanisms of selective autophagy in plants, we performed a yeast-two hybrid (Y2H) screening in the Arabidopsis cDNA library using AtATG8e (a representative of nine Arabidopsis ATG8 isoforms) as a bait. In the positive colonies, we found clones encoding FCS-like Zinc Finger protein 14 (AtFLZ14, At5g20700) (Fig 1A). We further checked the protein interactions between AtFLZ14 and other four typical ATG8 family members (AtATG8a, AtATG8d, AtATG8f and AtATG8g) and found that AtFLZ14 showed strong interaction with all these tested ATG8 family proteins in Y2H assay (Fig. 1A). The AtFLZ14-AtATG8e interaction was further confirmed by in vitro pull-down assay, which showed that His-MBP-AtFLZ14 could bind with GST-ATG8e but not with the control GST protein (Fig 1B). Protein sequence analysis revealed that AtFLZ14 contains a canonical EDYTLV sequence termed ATG8-interacting motif (AIM) and a conserved FLZ domain (Fig 1C). To determine whether AtFLZ14 binds to ATG8 via the canonical AIM-LDS (LIR/AIM docking site) interface (Noda et al., 2010), we constructed an AtFLZ14Y123AV126A with mutations of AIM motif and an AtATG8eY50AL51A with mutation of the LDS region for interaction assay (Fig 1C). The Y2H assay demonstrated that mutations of either AIM in AtFLZ14 or LDS in AtATG8e completely abolished their interactions (Fig 1D), indicating that the AIM-LDS interface indeed contributes to the association between AtFLZ14 and AtATG8. Further co-immunoprecipitation (Co-IP) assays also verified the interaction between AtFLZ14 and ATG8e and the requirement of AIM for their interactions in planta (Fig 1E).

Arabidopsis genome encodes 18 typical FLZ proteins (Fig S1A) (Jamsheer et al., 2015; Nietzsche et al., 2014). Protein sequence alignment showed that seven closely related AtFLZ proteins (AtFLZ8, 9, 10, 11, 12, 13 and 14) harbor the conserved AlM on the first β sheet of these AtFLZ proteins (Fig S1B and S2). The nature of AlM-LDS interface-mediated interaction between ATG8 and its substrates is a type of specific intermolecular β-sheet interaction (Noda et al., 2010), thus we wondered whether these AlM-containing FLZ proteins could bind to AtATG8. As expected, the Y2H assay showed that all members of these AlM-containing FLZ family, including AtFLZ8, 9, 10, 11, 12 and 13, could interact with AtATG8e (Fig S3). To examine whether the spatiotemporal activity of these AlM-containing AtFLZs and AtATG8e overlaps and meets the requirement for their interactions in vivo, we checked the gene expression profiles of them by using the Arabidopsis eFP browser, a visualization tool for exploring publicly available microarray data sets (Winter et al., 2007). As shown in Figure S4, all the seven AtFLZ

genes encoding AIM-containing AtFLZs displayed ubiquitous expression patterns, among them AtFLZ14 showing the highest expression, whose profile is largely overlapped with that of *AtATG8e*. Collectively, these results demonstrate that these seven AIM-containing FLZ proteins interact with ATG8 in Arabidopsis, indicating a molecular link between FLZ family proteins and autophagy pathway.

ATG8-interacted AtFLZs negatively regulate the tolerance of plants to long-term carbon starvation

The interactions between the aforementioned FLZ family proteins and ATG8 proteins motivated us to hypothesize that these FLZs proteins might be engaged in autophagy pathway by acting as either autophagic cargoes or modulators. To test the biological functions of these AtFLZ proteins, we selected four members (AtFLZ10, 11, 13 and 14) from different subclades (Fig S1A) to generate the transgenic Arabidopsis plants overexpressing AtFLZ genes under the control of Arabidopsis UBQ10 promoter (pUBQ10:AtFLZ-GFP, termed AtFLZ-OE). Reverse-transcription PCR (RT-PCR) analysis confirmed the overexpression of these AtFLZs in the corresponding transgenic plants (Fig 2A and S5). Considering that AtFLZs expression actively respond to energy deprivation (Jamsheer et al., 2015), we tested the response of these AtFLZ-OE plants to carbon starvation. Intriguingly, we found that all these AtFLZ-OE plants exhibited much higher sensitivity to carbon starvation with significantly lower survival rates in comparison with that of WT (Fig 2B, C and S5).

Since AtFLZ14 harbors the highest expression level and its overexpression in plants leads to most obvious sensitivity to fixed-carbon starvation among the FLZ genes in our testing (Fig S4A, 2B and C), we chose AtFLZ14 as an example to analyze its detail roles in the regulation of plant response to carbon starvation. To this end, we obtained a T-DNA insertion mutant of AtFLZ14 (designated flz14-1), which is a null mutant as no full-length transcript of AtFLZ14 was detected (Fig 2A and S6). Moreover, we also used CRISPR/Cas9 technology to obtain one AtFLZ14 gene edited line, termed flz14-2, with an insertion of one nucleotide in the genomic region that would create a pre-mature stop codon, thereby disrupting the function of AtFLZ14 (Fig S6). Interestingly, in contrary to the AtFLZ14-OE plants, both flz14-1 and flz14-2 mutants were relatively tolerant to fix-carbon starvation, as manifested by slightly higher survival rates when compared to that of WT (Fig 2B and C). We also introduced a construct containing the entire genomic sequence of AtFLZ14 into flz14-1 mutant and found that these complementary lines (gFLZ14 flz14-1 #5 and gFLZ14 flz14-1 #7) behaved like WT plants in response to fix-carbon starvation (Fig 2A-C), indicating that knockout of AtFLZ14 was indeed responsible for the carbon starvation-tolerance phenotype of flz14-1. Collectively, the above phenotypic data suggest that these ATG8-interacted AtFLZs members, including AtFLZ10, AtFLZ11, AtFLZ13 and AtFLZ14, negatively modulate the tolerance of plants to fix-carbon starvation.

Since AtFLZ14 interacts with AtATG8e and modulates plant carbon starvation resistance (Fig 1 and 2), we therefore inspired to test whether AtFLZ14 affects the activity of autophagy, a pathway critical for plant survival under carbon-limited conditions (Huang et al., 2019). We introduced pUBQ10:YFP-ATG8e (Gao et al., 2015) into flz14-1 mutant by crossing and monitored the formation of YFP-ATG8e-labeled autophagosomes in response to carbon starvation treatment. Under nutrient-rich growth conditions, both WT and flz14-1 seedlings had very few visible YPF-ATG8-decorated autophagosomes, and there was no significant difference in their numbers (Fig 2D), indicating that mutation of AtFLZ14 does not significantly affect the basal autophagy activity under nutrient-rich growth condition. YFP-ATG8e-lablled autophagosomes were easily observed in both WT and flz14-1 after 3 h of carbon starvation treatment (Fig 2 D), whereas more YFP-ATG8e puncta were found in flz14-1 mutant than that in WT (Fig 2 E). Concanamycin A (Conc A), an inhibitor of vacuolar H+-ATPase (Thompson et al., 2005), was added to the MS-C medium to inhibit the degradation of autophagic bodies inside vacuoles. As shown in Figure 2D and E, carbon starvation together with Conc A treatment boosted the detection of YFP-ATG8e-labeled autophagic vesicles in the central vacuoles of the root cells in both flz14-1 mutant and WT seedlings, whereas the flz14-1 mutant accumulated substantially more YFP-ATG8e puncta than that in WT plants, suggesting that AtFLZ14 negatively regulates autophagy under carbon starvation conditions.

To further confirm the negative regulatory action of AtFLZs on the autophagy induction in response to carbon starvation treatment, we obtained the transgenic plants co-expressing *pUBQ10:AtFLZ13/14* and *p35S:GFP-ATG8a* for detection of autophagy activity. As shown in Figure S7A and B, under normal conditions, the formation of *GFP-ATG8a* puncta showed no obvious difference in WT and *pUBQ10:AtFLZ13/14* backgrounds. However, compared to the WT, the *AtFLZ13/14* overexpressing plants accumulated less GFP-ATG8a puncta after 5 h of starvation combined with Conc A treatment, indicating that overexpression of AtFLZ14 decreases the autophagic activity (Fig S7A and B). Consistently, the GFP-ATG8a cleavage assay also verified that the autophagic flux was lower in the *AtFLZ13/14* overexpressing plants than WT controls (Fig S7C).

We next obtained a *flz14-1 atg7-2* double mutant by crossing *flz14-1* with *atg7-2*, an autophagy-defective mutant (Chung et al., 2010), and subjected these mutant plants to fix-carbon starvation analysis. As expected, the better tolerance of *flz14-1* mutant to long-term carbon starvation was completely abolished in *flz14-1 atg7-2* double mutant, which displayed similar sensitivity to *atg7-2* mutant (Fig 2F and G), suggesting that a

functional autophagy pathway is required for the tolerance of *flz14-1* to fix-carbon starvation. Taken together, these data revealed that ATG8-interacted AtFLZ proteins negatively regulate the activity of autophagy and the tolerance of plants in response long-term carbon starvation.

AtFLZ proteins attenuate AtSnRK1.1 activity by repressing its T-loop phosphorylation

FLZ proteins are characterized as the scaffolds for SnRK1 complex (Jamsheer et al., 2018), and SnRK1.1 positively regulates autophagy and plant carbon starvation tolerance (Chen et al., 2017; Soto-Burgos and Bassham, 2017). We thus hypothesized that the ATG8-interacted AtFLZ proteins might regulate autophagy and plant tolerance to energy starvation through affecting SnRK1 activity. AtSnRK1.1 contains three major domains including kinase, UBA and KA1 domains (Fig 3A). The kinase domain possesses the activation loop (T-loop), in which the phosphorylation of the conserved threonine (T^{T175}) is essential for its activity (Emanuelle et al., 2015; Williams et al., 2014). The UBA domain promotes and maintains T-loop phosphorylation (Emanuelle et al., 2018), whereas the KA1 domain involves in the dephosphorylation of T-loop (Broeckx et al., 2016; Rodrigues et al., 2013). We first mapped the interaction regions of SnRK1.1 with ATG8-interacted AtFLZs by performing Y2H assays with truncated proteins and found that all the tested four AtFLZs (AtFLZ10, 11, 13 and 14) showed strong interactions with the UBA domain (291-332 aa), but not with the kinase (1-271 aa) and KA1 (463-512 aa) domains (Fig 3B), opening a possibility that these AtFLZs might affect the T-loop phosphorylation of AtSnRK1.1.

To test this possibility, we transiently expressed AtSnRK1.1-GFP only or with AtSnAK2-6HA and AtFLZ-6HA in tobacco leaves and examined the protein accumulation and phosphorylation of AtSnRK1.1-GFP by immunoblotting with anti-GFP and anti-AMPKT¹⁷⁵ antibodies. The proteins of AtSnAK2-6HA and AtFLZ-6HA were well expressed, and they did not affect the expression and protein abundance of AtSnRK1.1-GFP (Fig 3C). Consistent with previous studies showing that AtSnAK2 functions as the upstream kinases of SnRK1 to phosphorylate the T-loop of SnRK1 α subunits (Glab *et al.*, 2017; Shen *et al.*, 2009), we also found that co-expression with AtSnAK2-6HA substantially enhanced the T¹⁷⁵ phosphorylation level of AtSnRK1.1-GFP (Fig 3C). Intriguingly, co-expression with AtFLZ10/11/13/14-6HA considerably reduced the T¹⁷⁵ phosphorylation level but not the total protein level of AtSnRK1.1-GFP (Fig 3C). We also transformed equal amount of AtSnRK1.1-YFP into *Arabidopsis* protoplasts with different amount AtFLZ14-6HA, and checked the protein levels of AtSnRK1-YFP. As

shown in Figure S8A, increasing amount of AtFLZ14-6HA did not obviously affect the AtSnRK1-YFP protein level.

One recent report proved that carbon starvation can promote the degradation of SnRK1.1 via 26S proteasomal pathway (Han et al., 2020). In our immunoblotting analysis, we also found a decreased protein level of SnRK1.1-GFP upon carbon starvation, whereas mutation of *AtFLZ14* did not affect AtSnRK1.1 degradation induced by carbon starvation (Fig S8B). These data strongly suggest that these ATG8-interacted FLZ proteins suppresses SnRK1.1 phosphorylation but might marginally affect the protein stability of AtSnRK1.1. To further clarify how these FLZ affect the phosphorylation of AtSnRK1.1, we analyzed the effects of AtFLZ10/11/13/14 on AtSnAK2-mediated T¹⁷⁵ phosphorylation of AtSnRK1.1. The obtained results showed that addition of AtFLZ-6HA greatly compromised the effect of AtSnAK2-mediated promotion of T-loop phosphorylation in AtSnRK1.1, while the AtSnRK1.1 protein levels were similar among those samples (Fig 3D). Collectively, these results clearly demonstrated that AtFLZ10/11/13/14 actively repress the T-loop phosphorylation of AtSnRK1.1.

We next sought to determine whether these AtFLZs can function to repress SnRK1 signaling. We employed the widely used dual-luciferase assay (DLA) to evaluate the effect of AtFLZ10, 11, 13 and 14 on the signaling output of SnRK1 by measuring the transcriptional activation activity of AtSnRK1.1 toward its downstream target gene DIN6 (Fig 3E). In line with the results showing in previous reports (Blanco et al., 2019; Crozet et al., 2016), addition of AtSnRK1.1-6HA could substantially activate the expression of DIN6 (Fig 3F). However, co-expression with AtFLZs-6HA significantly decreased the AtSnRK1.1-regulated transcriptional activation of DIN6 (Fig 3F), suggesting that these AtFLZs function as repressors of SnRK1 signaling. To reinforce this conclusion, we next tested the SnRK1 signaling in planta by performing dark treatment of 3-w-old plants followed by measurement of DIN6 expression as readout of SnRK1 signaling (Crozet et al., 2016). As expected, darkness treatment led to a strong up-regulation of DIN6 in WT plants, while this up-regulation was greatly attenuated in AtFLZ-OE plants, especially in the AtFLZ14-OE lines (Fig S9), further supporting the negative regulatory roles of these AtFLZs in SnRK1 signaling. In summary, these results clearly demonstrate that all of these four tested ATG8-interacted AtFLZ proteins (AtFLZ10, 11, 13 and 14) can bind to the UBA domain of SnRK1.1 and actively inhibit its T¹⁷⁵ phosphorylation, thereby attenuating the SnRK1 signaling.

A functional AtSnRK1.1 is required for AtFLZ14 activity in repressing autophagy and plant tolerance to carbon starvation

To further test the negative regulatory roles of the ATG8-interacted AtFLZs in SnRK1

signaling pathway, we examined the protein levels and T¹⁷⁵ phosphorylation of AtSnRK1.1 in the *flz14* mutants using anti-SnRK1.1 and anti-AMPK^{T175} antibodies. As shown in Figure 4A, the endogenous protein levels of AtSnRK1.1 in the two *flz14* mutants were similar to that in WT plants after 3 h starvation treatment, whereas the levels of T¹⁷⁵ phosphorylated AtSnRK1.1 protein were about two-fold accumulated in these two mutants, indicating that higher SnRK1 activity might be mainly attributed to the higher T¹⁷⁵ phosphorylation level in the *flz14* mutants. Consistently, the qRT-PCR results showed that the dark-induced expression of *DIN6* was higher in the *flz14* mutants than WT plants (Fig 4B). However, a combined depletion of AtSnRK1.1 largely compromised the induction of *DIN6* in *flz14-1* (Fig 4B), indicating that the enhanced SnRK1 signaling in *flz14-1* requires a functional AtSnRK1.1.

To determine whether AtFLZ14-regulated autophagy depends on the activity of AtSnRK1.1, we introduced pUBQ10:YFP-ATG8e into the snrk1.1 single (Soto-Burgos and Bassham, 2017) and flz14-1 snrk1.1 double-null mutants by crossing and observed the formation of autophagosome upon carbon starvation treatment in these mutant plants. Under normal conditions, there was no significant difference in the number of autophagosomes among the WT, flz14-1, snrk1.1 and flz14-1 snrk1.1 plants (Fig 4C and D). However, when performed carbon starvation or carbon starvation plus Conc A treatment for 3 h, flz14-1 displayed much more YFP-ATG8e-decrorated autophagic vesicles, while snrk1.1 harbored relatively less autophagic vesicles, in comparison to WT (Fig 4C and D). Moreover, the number of YFP-ATG8e puncta in flz14-1 snrk1.1 double mutant was significantly decreased than that in flz14-1 mutant (Fig 4C and 4D), suggesting the requirement of SnRK1.1 for the increased autophagy activity in flz14-1 mutant. To further clarify the genetic relationship between AtFLZ14 and SnRK1.1, we analyzed the survival rates of WT, flz14-1, snrk1.1 and flz14-1 snrk1.1 in response to carbon starvation. Consistent with the previous results (Fig 2B and C), the flz14-1 mutant showed increased tolerance to carbon starvation when compared with WT (Fig 4E and F). The snrk1.1 mutant displayed mildly decreased tolerance to carbon starvation with slightly lower survival rate than that of WT (Fig 4E and F). However, the flz14-1 snrk1.1 double mutant showed significantly decreased tolerance to carbon starvation in comparison to flz14-1 (Fig 4E and F). These phenotypic data confirm that AtFLZ14 functions upstream of AtSnRK1.1 to regulate autophagy and plant carbon starvation tolerance.

Carbon starvation represses the transcription of *AtFLZ* genes and promotes autophagic degradation of AtFLZs

The above data showed that AtFLZ10, 11, 13 and 14 interacts with AtATG8 (Fig 1 and S3) and negatively regulate SnRK1 signaling, autophagy activity and plant tolerance to carbon

starvation (Fig 2, 3 and S5). Therefore, we hypothesized that carbon starvation might lead to down-regulation of these AtFLZs to relieve its repression in SnRK1 signaling, thereby improving plant fitness to energy stress. To test this hypothesis, we first analyzed the gene expression of *AtFLZ10*, *11*, *13* and *14* upon carbon starvation. qRT-PCR assay revealed that their expression levels were decreased gradually following carbon starvation treatment and were downregulated 50%-80% after 24 h treatment (Fig 5A). The GUS staining assay using *pAtFLZ14-GUS* transgenic plants also showed that depletion of sucrose decreased the GUS activity obviously (Fig 5B). We then checked the protein expression of these AtFLZs in response to carbon starvation using our established *AtFLZ-OE* lines (Fig 2 and S5). Interestingly, we found that the protein levels of all these GFP fusions of AtFLZs, including AtFLZ10, AtFLZ11, AtFLZ13 and AtFLZ14, were also gradually diminished upon a time course of carbon starvation, though these FLZ-GFP fusions were driven by an *AtUBQ10* promoter (Fig 5C), indicating that carbon starvation destabilizes AtFLZ proteins.

Given the exist of interactions between AtFLZs and AtATG8s (Fig 1 and S3), we speculated that AtFLZ proteins might degrade via autophagy pathway. To test this hypothesis, we first examined the effect of Conc A, which functions as a V-ATPase inhibitor to attenuate protein degradation inside vacuole. As respected, addition of Conc A efficiently blocked the carbon starvation-induced decrease of FLZs-GFP fusions (Fig 5D), implying the vacuole degradation of these AtFLZ-GFP proteins. We next tested the possible role of autophagy in the regulation of AtFLZ13-GFP and AtFLZ14-GFP degradation by expressing these AtFLZ13-GFP and AtFLZ14-GFP in the autophagy deficient atg7-2 mutant and detected the AtFLZs-GFP protein levels upon carbon starvation. As shown in Figure 5D and E, 12 h carbon starvation treatment induced the decrease of AtFLZ13/14-GFP proteins in WT but not in atg7-2 mutant, suggesting that carbon starvation-induced degradation of AtFLZs-GFP proteins depends on a functional autophagy pathway.

ATG8-interacted AtFLZ proteins mainly localize to the mitochondria and traffic to the vacuole for degradation upon carbon starvation

To further explore the protein dynamics of these ATG8-interacted AtFLZ proteins in response to carbon starvation, we next performed confocal microscopic analysis of the subcellular localizations of these AtFLZs-GFP fusions. To our surprise, all these GFP fusions of AtFLZs, including AtFLZ10, AtFLZ11, AtFLZ13 and AtFLZ14, localized to punctate dots (Fig 6A and S10). To confirm their localizations, we crossed the *AtFLZs-GFP* plants with different marker lines including the mitochondrial marker mito-RFP, the *cis*-Golgi marker Man1-RFP and the trans-Golgi network (TGN) marker

VHAa1-RFP (Geldner et al., 2009) to observe their colocalizations. As shown in Figure S10 and S11, AtFLZs-GFP fully co-localized with the mitochondrial marker but not with the Golgi and TGN markers. Staining with mito-tracker dye further confirmed the mitochondrial localization of AtFLZ14-GFP (Fig 6A and S11C). To rule out the possible artifact in mislocalization of AtFLZs-GFP due to constitutive expression driven by the AtUBQ10 promoter, we generated a plant expressing gFLZ13-GFP that fuses GFP to the entire genomic sequence of AtFLZ13 containing the native promoter and regulatory elements. As shown in Figure S12, the mitochondrial localization of AtFLZ13-GFP was also observed, confirming the mitochondria localization of these AtFLZ proteins regardless of their expression levels.

We next performed carbon starvation to test its effects on the protein stability and subcellular localization of AtFLZ-GFP fusions. The obtained results showed that under normal condition, FLZs-GFP fusions localize to mitochondria and no GFP signals inside the central vacuoles were observed (Fig 6B). However, upon 24 h carbon starvation and Conc A treatment, the FLZs-GFP signals were easily detected inside the central vacuoles (Fig 6B and S13A), indicating that carbon starvation triggers the trafficking of AtFLZ13/14-GFP proteins to the vacuolar lumen. To test whether the carbon starvation-induced vacuolar transport of FLZs-GFP depends on canonical autophagy pathway, we used the previously established AtFLZ13/14-GFP atg7-2 plants (Fig 5E) for confocal microscopic analysis. We found that AtFLZ13-GFP and AtFLZ14-GFP were scarcely detected inside the vacuoles in atq7-2 mutant upon 24 h carbon starvation and Conc A treatment (Fig 6B and S13B), suggesting that autophagy pathway is required for the carbon starvation-induced vacuolar trafficking of AtFLZs proteins. We then crossed AtFLZ13/14-GFP with mCherry-ATG8f and analyzed their co-localization upon carbon starvation treatment. As shown in Figure 6C and S13C, AtFLZ13/14-GFP partially co-localized with mCherry-ATG8f inside vacuoles. Together with the immunoblotting data showing the autopagy-dependent degradation of FLZs-GFP (Fig 5E), these confocal microscopic data further reinforce the conclusion that these ATG8-interacted AtFLZ proteins are transported to vacuole for degradation through autophagy pathway in response to carbon starvation.

To check the subcellular locations where AtFLZ14 and AtSnRK1.1 interacts and to determine whether carbon starvation-induced degradation of FLZ14 affects its interaction with AtSnRK1.1, we next raised the transgenic plants stably co-expressing AtFLZ14-YN and AtSnRK1.1-YC for bimolecular fluorescence complementation (BiFC) assay. As shown in Figure 6D, under normal condition, strong punctate YFP signals were observed in the Arabidopsis root cells co-expressing AtFLZ14-YN and AtSnRK1.1-YC seedlings, but not in the negative control plants co-expressing AtFLZ14-YN and empty YC. Interestingly,

the reconstituted YFP signals were completely overlapped with the mitotracker-labeled mitochondrion (Fig 6D), suggesting that AtFLZ14 interacts with SnRK1.1 on mitochondria. We then checked the effect of carbon starvation on the interaction between AtFLZ14 and AtSnRK1.1, and found that the fluorescent intensities of both AtFLZ14-GFP and the reconstituted YFP signals resulting from AtFLZ14-YN and AtSnRK1.1-YC were obviously diminished after 12 h carbon starvation (Fig 6E), indicating that the carbon starvation-induced degradation of AtFLZ14 compromises the interaction between AtFLZ14 and SnRK1.1

The ATG8-FLZ-SnRK1 module is originated in gymnosperm and performs conserved functions in seed plants

SnRK1 and ATG8 are ubiquitously presented in green plants (Broeckx *et al.*, 2016; Seo et al., 2016), while FLZ protein is originated in bryophytes (Jamsheer *et al.*, 2015). To determine when the ATG8-FLZ-SnRK1 regulatory axis is formed during plant evolution, blast searches of publicly available genome sequence from *Chlamydomonas reinhardtii* (green algae), *Marchantia polymorpha* (bryophyte), *Selaginella moellendorffifii* (lycophyte), *Ceratopteris richardii* (monilophytes), *Picea abies* (gymnosperm) and four representative angiosperms (two monocots: *Zea mays* and *Oryza sativa*; two eudicots: *Arabidopsis thaliana* and *Solanum lycopersicum*) on Phytozome 13 (www.phytozome.jgi.doe.gov) were carried out. As shown in Fig 7A, we totally identified 20 SnRK1α proteins, 149 FLZ proteins and 37 ATG8 proteins, respectively, in these representative plant linages. SnRK1α and ATG8 were presented in all the examined plant genomes, and the number of them varied from 1 to 3 and 1 to 9, respectively (Fig 7A).

Consistent with the phylogenic analysis of FLZs in a previous report (Jamsheer *et al.*, 2015), we also did not find FLZ protein in *Chlamydomonas reinhardtii*, but identified one FLZ protein in the liverwort *Marchantia polymorpha* (Fig 7A), an ancestral land plant (Bowman et al., 2017), supporting a bryophytic origin of FLZ protein. The Y2H result showed that MpFLZ1 strongly interacted with MpSnRK1.1 but not with MpATG8 (Fig 7B), indicating that SnRK1-FLZ interaction module is first occurred in bryophytes and highly conserved throughout plant evolution (Chen et al., 2021; Ma et al., 2021; Nietzsche *et al.*, 2014). Interestingly, although *Ceratopteris richardii*, a widely investigated model fern specie (Marchant et al., 2019), has 23 FLZ proteins, whereas none of them possess the conserved ATG8-interacting motif (Fig 7A). The basal gymnosperm *Picea abies* (Nystedt et al., 2013) also contains 23 FLZ proteins and 8 of them harbor at least one conserved AIM motif (Fig 7A), indicating that AIM-containing FLZ proteins seems to be firstly emerged in gymnosperms. The four typical angiosperms encompass 5 to 8 AIM-containing FLZ proteins (Fig 7A). Collectively, these results indicated that

SnRK1-FLZ module is originated in bryophytes, while SnRK1-FLZ-ATG8 axis is firstly generated in gymnosperms and highly conserved during seed plant evolution.

Phylogenetic analysis revealed that the identified 149 FLZ proteins can be roughly divided into three subfamilies (Fig 7C). Interestingly, all the AIM-containing FLZ proteins from angiosperms belong to the subfamily III, while *Picea abies* AIM-containing FLZ proteins belong to the subfamily I (Fig 7C). Furthermore, the core AIM or LDS sequence and their surrounded residues were quite conserved (Fig 7D and E). To experimentally verify the conservation of FLZ-ATG8 interaction, we chose the orthologs of AtFLZ14 from maize (ZmFLZ14) and tomato (SIFLZ14) as examples to test their interactions with AtATG8e. We found that ZmFLZ14 and SIFLZ14 could interact with AtATG8e, but not with the AtATG8e with mutation of LSD motif in the Y2H assays (Fig 7F). These results further support that the ATG8-FLZ module is evolutionarily conserved in seed plants.

Since ZmFLZ14 interacts with AtATG8e (Fig 7E) and ZmSnRK1.1 (Chen et al., 2021), we therefore wondered whether ZmFLZ8 performs similar functions as that of AtFLZ14 in modulating plant response to plant carbon starvation. To this end, we first checked the expression patterns of ZmFLZ14, ZmATG8e and ZmSnRK1.1 and found that they displayed overlapping expression profiles in different maize tissues (Fig S15A), meeting the requirement of their interactions in vivo. Then, we examined the subcellular localization of ZmFLZ14 and verified that ZmFLZ14-GFP resides at mitochondrial in transgenic Arabidopsis plants under normal conditions (Fig S15B). Lastly, we used CRISPR/Cas9 technology to generate ZmFLZ14 gene edited lines and the three obtained lines (zmflz14-1, 6 and 10) respectively harbored a deletion of 2, 66 and 73 nucleotides that would create a pre-mature stop codon, thereby disrupting the function of ZmFLZ14 (Fig 8A). In the carbon starvation assay, all the three mutants showed better tolerance as manifested by much higher survival rates than the B104 wild-type plants (Fig 8B and C), suggesting that ZmFLZ14 functions similarly to AtFLZ14 in negatively regulating plant response to carbon starvation. Collectively, these data proved that the ATG8-FLZ-SnRK1 regulatory module is originated in gymnosperm and seems to function conservatively in seed plants.

DISCUSSION

Numerous studies in mammals and yeast have well established the critical roles of AMPK/SNF1 kinases in modulating autophagy activation (Saikia and Joseph, 2021). Several recent studies carried out in plants also uncovered the roles of SnRK1 in autophagy induction (Chen *et al.*, 2017; Huang *et al.*, 2019; Soto-Burgos and Bassham, 2017), indicating that the regulatory mechanisms of AMPK/SNF1/SnRK1 in autophagy pathway are conserved across kingdoms. Upon energy starvation, AMPK can rapidly

phosphorylate and activate ULK1/ATG1 to induce autophagy (Egan et al., 2011; Kim et al., 2011; Lee et al., 2010). Intriguingly, activated ULK1/ATG1 subsequently phosphorylates all three subunits of AMPK, leading to reduction levels of phosphorylation at T^{172} in the α subunits, thereby negatively regulating its activity (Loffler et al., 2011). In this work, we first demonstrate that autophagy contributes to the positive feedback regulation of SnRK1 signaling under carbon starvation conditions by mediating the selective degradation of SnRK1 repressors termed AIM-containing FLZ proteins. Under normal condition, these FLZ proteins are relative stable and interact with SnRK1 α subunits to decrease its T-loop phosphorylation, thereby preventing the hyper-activation of SnRK1 signaling and maintaining autophagy activity at a basal level. Upon energy starvation, SnRK1 is activated rapidly to induce autophagy, the activation of autophagy accelerates the degradation of these FLZ proteins to further release SnRK1 activity to enable survival.

As a major quality control pathway, selective autophagy can remove damaged or unwanted cargoes such as aggregated proteins, damaged or excess organelles, to maintain cellular homeostasis and to regulate plant stress response and developmental transition (Brillada et al., 2021; Li et al., 2020; Nolan et al., 2017; Stephani et al., 2020; Yang et al., 2018; Yang et al., 2019; Zhan et al., 2018; Zhang et al., 2020; Zhou et al., 2018). However, we are still far beyond a full understanding as to the regulations and functions of selective autophagy in plants, mostly because only few selective autophagy receptors (SARs) and their cargoes have been identified and functionally characterized (Liu et al., 2021; Stephani and Dagdas, 2020). In this study, we identified seven ATG8-interacted FLZ proteins and revealed that these AIM-containing FLZ proteins firstly appear in basal gymnosperm and are evolutionarily conserved during angiosperms (Fig 7A). Moreover, site-directed mutagenesis and cross-species interactions analysis (Fig 1E and 7F) confirmed that the ATG8-FLZ interaction relays the AIM-LDS interface and is highly conserved in seed plants. We also provided several strong evidences showing that these ATG8-interacted FLZ proteins are transported to vacuole for degradation through autophagy pathway during energy starvation (Fig 6B). Although we cannot ascertain whether these AtFLZ proteins function as SARs currently, our data illustrate the important roles of selective autophagy in AtFLZ proteins homeostasis. Given that several FLZ-interacting proteins have been identified in plants (Chen et al., 2021; Jamsheer et al., 2015; Nietzsche et al., 2016), it will be interesting to test whether they are regulated by FLZ-mediated selective autophagy.

FLZs is a class of plant specific C2-C2 zinc finger protein harboring a conserved FLZ domain (also known as DUF581). The FLZ domain is responsible for the interaction with $SnRK1\alpha$ subunits, whereas the intrinsically disordered regions (IDRs) in the N termini

facilitate interactions with the β and $\beta\gamma$ subunits of SnRK1 (Jamsheer *et al.*, 2018; Nietzsche et al., 2014). Most recently, the SnRK1-FLZ interaction module were experimentally verified in rice and maize (Chen et al., 2021; Ma et al., 2021). In this study, we further identified one FLZ protein in Marchantia polymorpha (Fig 7A), and confirmed that MpFLZ1 could also interact with MpSnRK1.1 (Fig 7B), indicating that SnRK1-FLZ module is originated in bryophytes and evolutionarily conserved in land plants. Since FLZ is a generic SnRK1 interaction module, it is generally considered as potential scaffold for SnRK1 complex in plants (Jamsheer et al., 2018; Nietzsche et al., 2014), but how FLZs modulate SnRK1 signaling has not been fully explored. In this work, we found that ATG8-interacted FLZ proteins could actively repress SnRK1 signaling by inhibition T-loop phosphorylation of AtSnRK1.1, rather than the protein level of ATSnRK1.1 (Fig 3 and 4). The results of DLA (Fig 3F) and qRT-PCR assay (Fig S9 and 4B) demonstrated that these FLZ proteins function as suppressors of SnRK1 signaling in Arabidopsis. Immunoblotting analysis using transiently expressed tobacco leaves (Fig 3) or Arabidopsis protoplast cells (Fig S8A) and transgenic Arabidopsis plants (Fig 4A and S8B) showed that overexpression or knockdown of ATG8-interacted FLZ genes did not affect the protein abundance of AtSnRK1.1, but obviously altered its T-loop phosphorylation. One recent report proved that carbon starvation can promote the degradation of AtSnRK1.1 via 26S proteasomal pathway (Han et al., 2020). Because carbon starvation can induce the trafficking of ATG8-interacted FLZ proteins to vacuole (Fig 6B), raising a possibility that these FLZ might serve as SARs to mediated the selective autophagy turnover of AtSnRK1.1 in vacuole. However, our data clearly showed that mutation of AtFLZ14 did not compromise carbon starvation induced AtSnRK1.1 degradation (Fig S8B). Furthermore, carbon starvation did not lead to vacuole trafficking of AtSnRK1.1-GFP (Fig S8C). Although we cannot exclude the possible involvement of these FLZ proteins in mediating autophagic degradation of SnRK1 β and/ or βγ subunits, which also interact with FLZ proteins (Jamsheer et al., 2018), our current data suggest that these FLZs regulate SnRK1 activity by affecting the T-loop phosphorylation, but not protein degradation, of SnRK1 α subunits.

It has been well established that SnRK1 kinase complex acts as an important cellular energy sensor, which can be activated by very diverse abiotic and biotic stress conditions that directly or indirectly cause an energy deficit (Crepin and Rolland, 2019), but how SnRK1 sense the cellular energy level remains not well understood. In mammals, energy currencies AMP and ATP can directly bind to the γ regulatory subunit of AMPK to antagonistically regulate its activity. AMP-binding promotes the phosphorylation or inhibits the dephosphorylation of AMPK at Thr¹⁷² and leads to allosteric activation of AMPK, while ATP-binding inhibit AMPK activity (Emanuelle et al., 2015; Li et al., 2015; Oakhill et al.,

2011; Xiao et al., 2011). However, unlike AMPK, SnRK1 is not allosterically activated by a relative increase in AMP level (Emanuelle et al., 2015; Ramon et al., 2013). In this study, unexpectedly, we found that under nutrient-rich condition, these ATG8-interacted FLZ proteins mainly localized to the mitochondria and interacted with AtSnRK1.1 on mitochondria, an organelle responsible for energy production within the cell. Interestingly, energy starvation induces the degradation of these FLZ proteins rapidly (Fig 5B and S14), thus attenuating SnRK1-FLZ association to relieve the repression of FLZ to SnRK1. Therefore, it is interesting to hypothesize that these FLZ proteins might serve as a bridge connecting the energy sensor SnRK1 and the energy reactor mitochondria, thereby letting SnRK1 complex directly and quickly sense cellular energy levels. Such a hypothesis is interesting to be tested in future works.

METHODS

Plant materials and growth conditions

All the *Arabidopsis thaliana* used in this study are Columbia (Col-0) background. The *flz14-1* T-DNA insertion mutant (SALK_060284C) was bought from Arabidopsis Biological Resource Center. The *atg7-2* (CS69859), *snrk1.1* (SALK_127939C), *p35S:GFP-ATG8a* and *pUBQ10:YFP-ATG8e* were previously reported (Chung *et al.*, 2010; Gao *et al.*, 2015; Soto-Burgos and Bassham, 2017; Yoshimoto et al., 2004). The *flz14-1 atg7-2* and *flz14-1 snrk1.1* double mutant were generated by crossing and genotyping. The *flz14-2* line was generated using the CRISPR/Cas9 system edited by two sequences of guide RNAs GTAGCAAGAAGTTGGGTAT and GTGTTTGAGTTCTCGAGCG following the previously established method (Xing et al., 2014). The *zmflz14* lines (*zmflz14-1/6/10*) were generated using the CRISPR/Cas9 system edited by two sequences of guide RNAs ATGACGTGCTTCAGGTCCAG and GTGCAGGGAACCGGTCCCGT following the previously reported method (Ishida et al., 2007; Xing *et al.*, 2014). The primers used were listed in Table S1.

To generate *AtFLZs*-, *ZmFLZ14*- and *AtSnRK1.1*-overexpressing plants, the full-length coding sequence of them were inserted into pCAMBIA1300 binary vector to in-frame fuse with a *Green Florescence Protein* (*GFP*) at the C-terminal driven by an *AtUBQ10* promoter. To generate the *gFLZ14 flz14* complementary lines, a genomic fragment of *AtFLZ14* containing a 2.0 kb promoter and the coding sequence was cloned into pCAMBIA1300 binary vector. To generate the *gFLZ13-GFP*, a genomic fragment of *AtFLZ13* containing a ~2.0 kb promoter and the coding sequence were inserted into pCAMBIA1300 binary vector to in-frame fuse with a *GFP* at the C-terminal. To generate the *pAtFLZ14-GUS*, a ~2.0 kb promoter region of *AtFLZ14* were cloned into the

pCAMBIA1391z to drive the expression of *GUS* reporter gene. The primers used were listed in Table S1. All the resulting constructs were transformed into *Agrobacterium tumefactions* GV3101 and then introduced into Wild-type (Col-0) or the indicated mutant plants using the floral dip method (Zhang et al., 2006).

All the seeds of Arabidopsis were surface sterilized with 30% (v/v) bleach for 5 min, washed with ddH₂O for 3 times (3 min each time), then kept at 4°C in the darkness for 3 d before being sown on standard MS medium plates supplemented with 0.8% (w/v) agar and 1% sucrose. After 7 d, the well-established seedlings were transferred to soil and grown in a chamber at 23°C under long-day conditions (LD, 16 h light/ 8 h dark). Seeds of maize were surface sterilized with 30% (v/v) bleach for 5 min, washed with ddH₂O for 3 times, then directly planted in soil and grown in a chamber at 28°C under LD conditions.

Protein-protein interaction assays

For yeast two hybrid assay, the full-length, truncated or mutated version of the indicated genes were cloned into the pGADT7 or pGBKT7 vectors, respectively. The primers used were listed in Table S1. Then the different combinations of plasmids were transformed into following the manufacturer's yeast stain AH109 instructions (Clontech, http://www.clontech.com/). Finally, the protein interaction was determined by growth of the yeast cells co-transformed with different plasmid combinations on synthetic dropout medium lacking Leu and Trp (SD-LW), and synthetic dropout medium lacking Leu, Trp and His (SD-LWH), or synthetic dropout medium lacking Leu, Trp, His, and adenine (SD-LWHA) for 3 to 5 d after planting.

For *in vitro* pull-down assay, the full-length coding sequence of *AtFLZ14* and *AtATG8e* were cloned into pMAL-c2x and pGEX4T-3 vectors, respectively. The primers used were listed in Table S1. Then, the resulting vectors were transformed into *E. coli* BL21 (DE3) to express His-MBP-AtFLZ14 and GST-AtATG8e fusion proteins at 25°C for 6 h induction with 0.4 mM IPTG. Equal volume supernatant containing His-MBP-AtFLZ14 proteins were incubated with GST and GST-AtATG8e pre-bound to glutathione agarose beads with gentle rotation at 4°C for 4 h. After washing 6 times with 1 ml PBS, the beads were boiled for 10 min in 100 µl 1×SDS-PAGE loading buffer. Finally, the presence of GST-tagged and His-MBP-tagged proteins was detected by immunoblotting using anti-His (BoAo) and anti-GST (BoAo) antibodies.

For co-immunoprecipitation assay, *p35S:FLZ14-6HA* or *p35S:FLZ14*^{Y123AV126A}-6HA were transiently co-expressed with *pUBQ10:YFP* or *pUBQ10:YFP-ATG8e* in Arabidopsis protoplasts as indicated. After incubation in darkness for 12 h, the cells were harvested for protein extraction with 2 ml ice-cold lysis buffer (30 mM Tris-HCl, pH 7.4, 300 mM NaCl, 1 mM EDTA, 20% glycerol, 1 mM PMSF, 0.2% (v/v) NP-40, and protease inhibitor cocktail).

Immunoprecipitation was conducted with GFP-Trap Magnetic Agarose for 3 h with gentle rotation at 4°C according to the manufacturer's instructions (Chromotek, https://www.chromotek.com/). Finally, the protein samples were separated by 10% SDS-PAGE and the fusion proteins were detected with anti-HA (Abcam) and anti-GFP (Abcam) antibodies.

For bimolecular fluorescence complementation assay, the full-length coding sequence of *AtFLZ14* was cloned into the pCAMBIA1300-YN vector to produce *AtFLZ14-YN*, while *AtSnRK1.1* was cloned into pCAMBIA1300-YC to produce *AtSnRK1.1-YC*. The primers used were listed in Table S1. Then, the resulting constructs were transformed into *Agrobacterium tumefactions* GV3101 and then introduced into Wild-type (Col-0) using the floral dip method (Zhang *et al.*, 2006). For the interaction detection, the progeny of crossed F1 were used to observe with a Zeiss 800 Laser scanning confocal microscope.

Data search and analyses

Identification of FLZ, SnRK1 and ATG8 proteins in rice and maize were performed as previously described (Chen et al., 2021; Ma et al., 2021), while identification of them in Picea abies were conducted on ConGenIE (Conifer Genome Integrative Explorer) web resource (http://congenie.org). To identify the FLZ, SnRK1 and ATG8 proteins in other specifies as shown in Figure 7A, we downloaded the protein sequences from Phytozome V13 (https://phytozome-next.jqi.doe.gov/) and screened the homologous proteins by a local blast program using the protein sequence of FLZ-domain of AtFLZ14 and the full-length of AtSnRK1.1 and AtATG8e as gueries with a p-value < 0.001. A phylogenetic tree of 149 AtFLZ proteins based on amino acid sequences was constructed using the Maximum Likelihood method based on the JTT matrix-based model. The tree with the highest log likelihood (-3426.6125) is shown. All positions containing gaps and missing data were eliminated. Evolutionary analyses were conducted in MEGA5.0. The sequence logs regarding to FLZ-AIM and ATG8-LDS were generated by MEME web server (https://meme-suite.org/meme/tools/meme) using the conserved sequence of them from the 36 AIM-containing FLZ proteins and 35 LDS-containing ATG8 proteins, respectively. To analyze the expression patterns of representative ATG8, FLZ and SnRK1 genes, the expression data were downloaded from BAR (http://bar.utoronto.ca/) using the locus ID as queries. The protein structure of AtFLZs and AtATG8e were retrieved and downloaded from AlphaFold DB (https://alphafold.ebi.ac.uk/) using the locus ID as queries.

Long-term fix-carbon starvation assay

Fix-carbon starvation assay for Arabidopsis was carried out as our previously established

method (Li et al., 2022). Briefly, Arabidopsis seeds was surface sterilized and kept at 4 °C in darkness for 2 d before being sown on solid MS-C (without sucrose) medium plates for germination and growth under LD conditions. Subsequently, 14-day-old seedlings were completely wrapped by tinfoil to keep continuous darkness for 11 to 13 d, and then transferred back to LD conditions. After 5-7 days' recovery growth, the plates were photographed with a digital camera and the survival rates were calculated. Carbon starvation treatment for maize was carried out as follow: 15-day-old seedling in soil were exposed to dark for 80 h, then transferred back to LD condition of recovery growth for 5 d before being taken pictures and the survival rates were calculated.

Dual-luciferase assay

Dual-luciferase reporter assay was carried out as previously described (Yang et al., 2018). Briefly, the full-length coding sequence of AtSnRK1.1 was cloned into the pSAT6-eYFP-N1 vector, and the full-length coding sequences of AtSnAK2 or AtFLZs were separately cloned into p35S:6HA vector, to express the effectors. A 2.0 kb promoter region of AtDIN6 was inserted into the pGreenII 0800-LUC to produce the reporter vector. The primers used were listed in Table S1. Different plasmid combinations as indicated were used for Arabidopsis protoplast transfection. After incubation in darkness for 12 h, the protoplasts were harvested to isolate total protein for LUC (Luciferase) and REN (Renilla luciferase) activity detection using a dual-luciferase reporter assay system kit (Promega E1910) with a luminometer. Relative Luciferase Activity was calculated as LUC/REN.

Transient expression assays in tobacco leaves or Arabidopsis suspension cells

To check the effects of AtSnAK2 and AtFLZs on the protein expression or phosphorylation modification of SnRK1.1, *pUBQ10:SnRK1.1-GFP* were transiently co-expressed in 4-week-old *N. benthamiana* leaves with *p35S:AtSnAK2-6HA* and *p35S:AtFLZs-6HA*, respectively, and the total proteins were extracted 3 d after Agrobacterium infiltration for immunoblotting using Anti-AMPKT175 (Agrisera), Anti-GFP (Abcam) and anti-HA (Abcam) antibodies. Ponceau staining denotes protein loading.

To analyze the effect of AtFLZ14 on the protein expression of SnRK1.1, equal amount SnRK1.1-eYFP plasmid (100 μ g) were separately co-transfected with 0, 30, 60 and 120 μ g AtFLZ14-6HA plasmid into Arabidopsis suspension cells as previously described (Gao et al., 2014), then the transformed cells were incubated in darkness for 12 h before being harvested to extract total protein for immunoblotting using Anti-GFP (Abcam) and Anti-HA (Abcam) antibodies. CBB staining denotes the protein loading.

Proteins extraction from Arabidopsis and immunoblotting

To analyze the protein levels of AtFLZ-GFP following carbon starvation treatment, 5-d-old seedlings grown on MS medium plates under LD conditions were transferred to MS-C liquid medium with or without 1 μ m Conc A and kept in darkness for 0, 3, 6, 12 and 24 h before being harvested to extract total proteins. The total proteins were extracted from the harvested seedlings using 2 × SDS-PAGE sample buffers (125 mM Tris-HCl (pH 6.8), 5% SDS, 20% glycerol, and 10% 2-mercaptoethanol) as described previously (Yang et al., 2020). Finally, the protein samples were subjected to 10% SDS-PAGE and immunoblotted with anti-GFP (Abcam) and Anti-UGPase (BoAo) antibodies.

To analyze the protein levels of AtSnRK1.1 in WT and *flz14-1* mutant plants, 5-d-old seedlings grown on MS medium plates under LD conditions were transferred to MS-C liquid medium in darkness for 3 h before being harvested to extract total proteins as described above. Finally, the protein samples were subjected to 10% SDS-PAGE and immunoblotted with anti-KIN10 (Agrisera), Anti-AMPKT175 (Agrisera) and Anti-FBPase (Abcam) antibodies.

RNA extraction and gene expression analysis

The total RNA was isolated from the harvested samples using a Hipure plant RNA Mini kit (Magen). Total RNA (about 500 ng) was reverse-transcribed using HiScript \square Q Select RT SuperMix (Vazyme), and the resulting first strand cDNA was used as template for quantitative real-time PCR (qRT-PCR) or semiquantitative reverse transcription PCR (RT-PCR) analysis. qRT-PCR was performed using iTaqTM Universal SYBR Green Supermix (Bio-Rad). The expression of *AtUBQ10* was used as an internal control and the relative expression was calculated using the $2^{-\triangle\triangle^{CT}}$ method. The primers used are listed in Table S1.

GUS staining was performed according to the method as described (Yang et al., 2018). Seedlings of the *pAtFLZ14:GUS* transgenic plants were incubated in a solution containing 50 mM NaPO4 buffer pH 7.0, 5 mM K3Fe(CN)₆, 5 mM K4Fe(CN)₆, 0.1% Triton X-100 and 1 mM X-Gluc at 37°C for 2 h. Images were taken under the stereo microscope (Leica).

Seedling treatment and confocal microscopy observation

Microscopy analysis of YFP-ATG8e. Five-day-old *pUBQ10:YFP-ATG8e* seedlings in WT, *flz14-1*, *snrk1.1* and *flz14-1 snrk1.1* backgrounds or *p35S:YFP-ATG8a* seedlings WT, *pUBQ10:AtFLZ13* and *pUBQ10:AtFLZ14* backgrounds grown on MS medium plates under LD conditions were transferred to MS-C liquid medium with or without 1 μM Conc A for 0 or 3/5 h in darkness. Root epidermal cells at the elongation zone were imaged using an LSM800 confocal microscope with a ×20 objective. The excitation and emission wavelengths for YFP were 488 and 507-550 nm, respectively.

Subcellular localization analysis of FLZ-GFPs. Five-day-old pBUQ10:AtFLZ14-GFP, pUBQ10:ZmFLZ14-GFP and gFLZ13-GFP Arabidopsis seedlings grown on MS medium plates under LD conditions were pre-stained with 500 nm TMRE for 5 min, then subjected to Zeiss LSM 880 confocal fluorescence microscopy observation with a ×63 oil immersion objective. The roots and cotyledons of the 5-day-old AtFLZ-GFP mito-RFP/VHA-a1-RFP/man1-RFP seedlings grown on MS medium plates under LD conditions were directly subjected to Zeiss LSM 880 confocal fluorescence microscopy observation with a ×63 oil immersion objective. Five-day-old AtFLZ-GFP13/14 × mCherry-VAMP711 seedling grown on MS medium plates under LD conditions were exposed to MS-C liquid medium containing 1 µm Conc A for 0 or 24 h before being observed with a Zeiss LSM 880 confocal fluorescence microscopy with a ×63 oil immersion objective. Five-day-old AtFLZ-GFP13/14 × mCherry-ATG8f seedlings grown on MS medium plates under LD conditions were exposed to MS-C liquid medium containing 1 µm Conc A for 24 h before being observed with a Zeiss LSM 880 confocal fluorescence microscopy with a ×63 oil immersion objective. Five-day-old AtFLZ-GFP13/14 atg7-2 seedlings grown on MS medium plates under LD conditions were exposed to MS-C liquid medium containing 5 µm FM4-64 for 6 h, then were incubated with 1 µm Conc A for another 12 h before being imaged with a Zeiss LSM 880 confocal fluorescence microscopy with a ×63 oil immersion objective. The excitation and emission wavelengths for GFP were 488 and 500-550 nm, respectively. The excitation and emission wavelengths for RFP, mCherry and FM4-64 were 561 and 585-650 nm, respectively.

Data processing and statistical analysis

The histograms were constructed by GraphPad Prism 5.0 software (http://www.graphpad.com) with the average values and standard deviation, and the original data were given in Table S2. Statistical differences were calculated by one-way ANOVA in SPSS program (https://spssau.com/) or Student's t-test in Microsoft Excel. Different letters indicate means that were statistically different by Tukey's multiple testing methods (P < 0.05). *P < 0.05, *P < 0.01.

REFERENCES

Ananieva, E.A., Gillaspy, G.E., Ely, A., Burnette, R.N., and Erickson, F.L. (2008). Interaction of the WD40 domain of a myoinositol polyphosphate 5-phosphatase with SnRK1 links inositol, sugar, and stress signaling. Plant Physiol **148**:1868-1882. 10.1104/pp.108.130575.

Baena-Gonzalez, E., Rolland, F., Thevelein, J.M., and Sheen, J. (2007). A central integrator of transcription networks in plant stress and energy signalling. Nature **448**:938-942. 10.1038/nature06069.

Blanco, N.E., Liebsch, D., Guinea Diaz, M., Strand, A., and Whelan, J. (2019). Dual and dynamic

intracellular localization of Arabidopsis thaliana SnRK1.1. J Exp Bot 70:2325-2338. 10.1093/jxb/erz023.

Bowman, J.L., Kohchi, T., Yamato, K.T., Jenkins, J., Shu, S., Ishizaki, K., Yamaoka, S., Nishihama, R., Nakamura, Y., Berger, F., et al. (2017). Insights into Land Plant Evolution Garnered from the Marchantia polymorpha Genome. Cell **171**:287-304 e215. 10.1016/j.cell.2017.09.030.

Brillada, C., Teh, O.K., Ditengou, F.A., Lee, C.W., Klecker, T., Saeed, B., Furlan, G., Zietz, M., Hause, G., Eschen-Lippold, L., et al. (2021). Exocyst subunit Exo70B2 is linked to immune signaling and autophagy. Plant Cell 33:404-419. 10.1093/plcell/koaa022.

Broeckx, T., Hulsmans, S., and Rolland, F. (2016). The plant energy sensor: evolutionary conservation and divergence of SnRK1 structure, regulation, and function. J Exp Bot **67**:6215-6252. 10.1093/jxb/erw416.

Chen, L., Su, Z.Z., Huang, L., Xia, F.N., Qi, H., Xie, L.J., Xiao, S., and Chen, Q.F. (2017). The AMP-Activated Protein Kinase KIN10 Is Involved in the Regulation of Autophagy in Arabidopsis. Front Plant Sci 8:1201. 10.3389/fpls.2017.01201.

Chen, S., Li, X., Yang, C., Yan, W., Liu, C., Tang, X., and Gao, C. (2021). Genome-wide Identification and Characterization of FCS-Like Zinc Finger (FLZ) Family Genes in Maize (Zea mays) and Functional Analysis of ZmFLZ25 in Plant Abscisic Acid Response. Int J Mol Sci **22**10.3390/ijms22073529.

Chung, T., Phillips, A.R., and Vierstra, R.D. (2010). ATG8 lipidation and ATG8-mediated autophagy in Arabidopsis require ATG12 expressed from the differentially controlled ATG12A AND ATG12B loci. Plant J **62**:483-493. 10.1111/j.1365-313X.2010.04166.x.

Coello, P., and Martinez-Barajas, E. (2014). The activity of SnRK1 is increased in Phaseolus vulgaris seeds in response to a reduced nutrient supply. Front Plant Sci **5**:196. 10.3389/fpls.2014.00196.

Crepin, N., and Rolland, F. (2019). SnRK1 activation, signaling, and networking for energy homeostasis. Curr Opin Plant Biol **51**:29-36. 10.1016/j.pbi.2019.03.006.

Crozet, P., Margalha, L., Butowt, R., Fernandes, N., Elias, C.A., Orosa, B., Tomanov, K., Teige, M., Bachmair, A., Sadanandom, A., et al. (2016). SUMOylation represses SnRK1 signaling in Arabidopsis. Plant J 85:120-133. 10.1111/tpj.13096.

Egan, D.F., Shackelford, D.B., Mihaylova, M.M., Gelino, S., Kohnz, R.A., Mair, W., Vasquez, D.S., Joshi, A., Gwinn, D.M., Taylor, R., et al. (2011). Phosphorylation of ULK1 (hATG1) by AMP-activated protein kinase connects energy sensing to mitophagy. Science **331**:456-461. 10.1126/science.1196371.

Emanuelle, S., Doblin, M.S., Gooley, P.R., and Gentry, M.S. (2018). The UBA domain of SnRK1 promotes activation and maintains catalytic activity. Biochem Biophys Res Commun **497**:127-132. 10.1016/j.bbrc.2018.02.039.

Emanuelle, S., Hossain, M.I., Moller, I.E., Pedersen, H.L., van de Meene, A.M., Doblin, M.S., Koay, A., Oakhill, J.S., Scott, J.W., Willats, W.G., et al. (2015). SnRK1 from Arabidopsis thaliana is an atypical AMPK. Plant J 82:183-192. 10.1111/tpj.12813.

Fragoso, S., Espindola, L., Paez-Valencia, J., Gamboa, A., Camacho, Y., Martinez-Barajas, E., and Coello, P. (2009). SnRK1 isoforms AKIN10 and AKIN11 are differentially regulated in Arabidopsis plants under phosphate starvation. Plant Physiol **149**:1906-1916. 10.1104/pp.108.133298.

Gao, C., Zhuang, X., Cui, Y., Fu, X., He, Y., Zhao, Q., Zeng, Y., Shen, J., Luo, M., and Jiang, L. (2015). Dual roles of an Arabidopsis ESCRT component FREE1 in regulating vacuolar protein transport and autophagic degradation. Proc Natl Acad Sci U S A **112**:1886-1891. 10.1073/pnas.1421271112.

Geldner, N., Dénervaud-Tendon, V., Hyman, D.L., Mayer, U., Stierhof, Y.D., and Chory, J. (2009). Rapid, combinatorial analysis of membrane compartments in intact plants with a multicolor marker set. Plant J **59**:169-178. 10.1111/j.1365-313X.2009.03851.x.

- Glab, N., Oury, C., Guerinier, T., Domenichini, S., Crozet, P., Thomas, M., Vidal, J., and Hodges, M. (2017). The impact of Arabidopsis thaliana SNF1-related-kinase 1 (SnRK1)-activating kinase 1 (SnAK1) and SnAK2 on SnRK1 phosphorylation status: characterization of a SnAK double mutant. Plant J 89:1031-1041. 10.1111/tpj.13445.
- Han, C., Liu, Y., Shi, W., Qiao, Y., Wang, L., Tian, Y., Fan, M., Deng, Z., Lau, O.S., De Jaeger, G., et al. (2020). KIN10 promotes stomatal development through stabilization of the SPEECHLESS transcription factor. Nat Commun 11:4214. 10.1038/s41467-020-18048-w.
- Huang, X., Zheng, C., Liu, F., Yang, C., Zheng, P., Lu, X., Tian, J., Chung, T., Otegui, M.S., Xiao, S., et al. (2019). Genetic Analyses of the Arabidopsis ATG1 Kinase Complex Reveal Both Kinase-Dependent and Independent Autophagic Routes during Fixed-Carbon Starvation. Plant Cell **31**:2973-2995. 10.1105/tpc.19.00066.
- **Ishida, Y., Hiei, Y., and Komari, T.** (2007). Agrobacterium-mediated transformation of maize. Nat Protoc **2**:1614-1621. 10.1038/nprot.2007.241.
- Jamsheer, K.M., Mannully, C.T., Gopan, N., and Laxmi, A. (2015). Comprehensive Evolutionary and Expression Analysis of FCS-Like Zinc finger Gene Family Yields Insights into Their Origin, Expansion and Divergence. PLoS One **10**:e0134328. 10.1371/journal.pone.0134328.
- Jamsheer, K.M., Shukla, B.N., Jindal, S., Gopan, N., Mannully, C.T., and Laxmi, A. (2018). The FCS-like zinc finger scaffold of the kinase SnRK1 is formed by the coordinated actions of the FLZ domain and intrinsically disordered regions. J Biol Chem **293**:13134-13150. 10.1074/jbc.RA118.002073.
- Jossier, M., Bouly, J.P., Meimoun, P., Arjmand, A., Lessard, P., Hawley, S., Grahame Hardie, D., and Thomas, M. (2009). SnRK1 (SNF1-related kinase 1) has a central role in sugar and ABA signalling in Arabidopsis thaliana. Plant J **59**:316-328. 10.1111/j.1365-313X.2009.03871.x.
- Kim, J., Kundu, M., Viollet, B., and Guan, K.L. (2011). AMPK and mTOR regulate autophagy through direct phosphorylation of Ulk1. Nat Cell Biol 13:132-141. 10.1038/ncb2152.
- Lee, J.W., Park, S., Takahashi, Y., and Wang, H.G. (2010). The association of AMPK with ULK1 regulates autophagy. PLoS One 5:e15394. 10.1371/journal.pone.0015394.
- Li, X., Liu, Q., Feng, H., Deng, J., Zhang, R., Wen, J., Dong, J., and Wang, T. (2020). Dehydrin MtCAS31 promotes autophagic degradation under drought stress. Autophagy **16**:862-877. 10.1080/15548627.2019.1643656.
- Li, X., Liao, J., Bai, H., Bei, J., Li, K., Luo, M., Shen, W., Yang, C., and Gao, C. (2022). Arabidopsis flowering integrator SOC1 transcriptionally regulates autophagy in response to long-term carbon starvation. J Exp Bot **73**:6589-6599. 10.1093/jxb/erac298.
- Li, X., Wang, L., Zhou, X.E., Ke, J., de Waal, P.W., Gu, X., Tan, M.H., Wang, D., Wu, D., Xu, H.E., et al. (2015). Structural basis of AMPK regulation by adenine nucleotides and glycogen. Cell Res **25**:50-66. 10.1038/cr.2014.150.
- **Liu, W., Liu, Z., Mo, Z., Guo, S., Liu, Y., and Xie, Q.** (2021). ATG8-Interacting Motif: Evolution and Function in Selective Autophagy of Targeting Biological Processes. Front Plant Sci **12**:783881. 10.3389/fpls.2021.783881.
- Loffler, A.S., Alers, S., Dieterle, A.M., Keppeler, H., Franz-Wachtel, M., Kundu, M., Campbell, D.G., Wesselborg, S., Alessi, D.R., and Stork, B. (2011). Ulk1-mediated phosphorylation of AMPK constitutes a negative regulatory feedback loop. Autophagy **7**:696-706. 10.4161/auto.7.7.15451.
- Ma, Y., Zhao, J., Fu, H., Yang, T., Dong, J., Yang, W., Chen, L., Zhou, L., Wang, J., Liu, B., et al. (2021). Genome-Wide Identification, Expression and Functional Analysis Reveal the Involvement of FCS-Like Zinc Finger Gene Family in Submergence Response in Rice. Rice (N Y) 14:76.

10.1186/s12284-021-00519-3.

Marchant, D.B., Sessa, E.B., Wolf, P.G., Heo, K., Barbazuk, W.B., Soltis, P.S., and Soltis, D.E. (2019). The C-Fern (Ceratopteris richardii) genome: insights into plant genome evolution with the first partial homosporous fern genome assembly. Sci Rep 9:18181. 10.1038/s41598-019-53968-8.

Margalha, L., Valerio, C., and Baena-Gonzalez, E. (2016). Plant SnRK1 Kinases: Structure, Regulation, and Function. Exp Suppl 107:403-438. 10.1007/978-3-319-43589-3_17.

Marshall, R.S., and Vierstra, R.D. (2018). Autophagy: The Master of Bulk and Selective Recycling. Annu Rev Plant Biol **69**:173-208. 10.1146/annurev-arplant-042817-040606.

Nietzsche, M., Schiessl, I., and Bornke, F. (2014). The complex becomes more complex: protein-protein interactions of SnRK1 with DUF581 family proteins provide a framework for cell- and stimulus type-specific SnRK1 signaling in plants. Front Plant Sci **5**:54. 10.3389/fpls.2014.00054.

Nietzsche, M., Landgraf, R., Tohge, T., and Börnke, F. (2016). A protein–protein interaction network linking the energy-sensor kinase SnRK1 to multiple signaling pathways in Arabidopsis thaliana. Current Plant Biology **5**:36-44. 10.1016/j.cpb.2015.10.004.

Noda, N.N., Ohsumi, Y., and Inagaki, F. (2010). Atg8-family interacting motif crucial for selective autophagy. FEBS Lett **584**:1379-1385. 10.1016/j.febslet.2010.01.018.

Nolan, T.M., Brennan, B., Yang, M., Chen, J., Zhang, M., Li, Z., Wang, X., Bassham, D.C., Walley, J., and Yin, Y. (2017). Selective Autophagy of BES1 Mediated by DSK2 Balances Plant Growth and Survival. Dev Cell **41**:33-46 e37. 10.1016/j.devcel.2017.03.013.

Nystedt, B., Street, N.R., Wetterbom, A., Zuccolo, A., Lin, Y.C., Scofield, D.G., Vezzi, F., Delhomme, N., Giacomello, S., Alexeyenko, A., et al. (2013). The Norway spruce genome sequence and conifer genome evolution. Nature **497**:579-584. 10.1038/nature12211.

Oakhill, J.S., Steel, R., Chen, Z.P., Scott, J.W., Ling, N., Tam, S., and Kemp, B.E. (2011). AMPK is a direct adenylate charge-regulated protein kinase. Science **332**:1433-1435. 10.1126/science.1200094.

Ramon, M., Ruelens, P., Li, Y., Sheen, J., Geuten, K., and Rolland, F. (2013). The hybrid four-CBS-domain KINbetagamma subunit functions as the canonical gamma subunit of the plant energy sensor SnRK1. Plant J **75**:11-25. 10.1111/tpj.12192.

Robertlee, J., Kobayashi, K., Suzuki, M., and Muranaka, T. (2017). AKIN10, a representative Arabidopsis SNF1-related protein kinase 1 (SnRK1), phosphorylates and downregulates plant HMG-CoA reductase. FEBS Lett **591**:1159-1166. 10.1002/1873-3468.12618.

Rodrigues, A., Adamo, M., Crozet, P., Margalha, L., Confraria, A., Martinho, C., Elias, A., Rabissi, A., Lumbreras, V., Gonzalez-Guzman, M., et al. (2013). ABI1 and PP2CA phosphatases are negative regulators of Snf1-related protein kinase1 signaling in Arabidopsis. Plant Cell **25**:3871-3884. 10.1105/tpc.113.114066.

Saikia, R., and Joseph, J. (2021). AMPK: a key regulator of energy stress and calcium-induced autophagy. J Mol Med (Berl) 99:1539-1551. 10.1007/s00109-021-02125-8.

Seo, E., Woo, J., Park, E., Bertolani, S.J., Siegel, J.B., Choi, D., and Dinesh-Kumar, S.P. (2016). Comparative analyses of ubiquitin-like ATG8 and cysteine protease ATG4 autophagy genes in the plant lineage and cross-kingdom processing of ATG8 by ATG4. Autophagy 12:2054-2068. 10.1080/15548627.2016.1217373.

Shen, W., Reyes, M.I., and Hanley-Bowdoin, L. (2009). Arabidopsis protein kinases GRIK1 and GRIK2 specifically activate SnRK1 by phosphorylating its activation loop. Plant Physiol **150**:996-1005. 10.1104/pp.108.132787.

Soto-Burgos, J., and Bassham, D.C. (2017). SnRK1 activates autophagy via the TOR signaling pathway

- in Arabidopsis thaliana. PLoS One **12**:e0182591. 10.1371/journal.pone.0182591.
- **Stephani, M., and Dagdas, Y.** (2020). Plant Selective Autophagy-Still an Uncharted Territory With a Lot of Hidden Gems. J Mol Biol **432**:63-79. 10.1016/j.jmb.2019.06.028.
- Stephani, M., Picchianti, L., Gajic, A., Beveridge, R., Skarwan, E., Sanchez de Medina Hernandez, V., Mohseni, A., Clavel, M., Zeng, Y., Naumann, C., et al. (2020). A cross-kingdom conserved ER-phagy receptor maintains endoplasmic reticulum homeostasis during stress. Elife **9**10.7554/eLife.58396.
- **Thompson, A.R., Doelling, J.H., Suttangkakul, A., and Vierstra, R.D.** (2005). Autophagic nutrient recycling in Arabidopsis directed by the ATG8 and ATG12 conjugation pathways. Plant Physiol **138**:2097-2110. 10.1104/pp.105.060673.
- Tome, F., Nagele, T., Adamo, M., Garg, A., Marco-Llorca, C., Nukarinen, E., Pedrotti, L., Peviani, A., Simeunovic, A., Tatkiewicz, A., et al. (2014). The low energy signaling network. Front Plant Sci 5:353. 10.3389/fpls.2014.00353.
- Williams, S.P., Rangarajan, P., Donahue, J.L., Hess, J.E., and Gillaspy, G.E. (2014). Regulation of Sucrose non-Fermenting Related Kinase 1 genes in Arabidopsis thaliana. Front Plant Sci 5:324. 10.3389/fpls.2014.00324.
- Winter, D., Vinegar, B., Nahal, H., Ammar, R., Wilson, G.V., and Provart, N.J. (2007). An "Electronic Fluorescent Pictograph" browser for exploring and analyzing large-scale biological data sets. PLoS One 2:e718. 10.1371/journal.pone.0000718.
- Xiao, B., Sanders, M.J., Underwood, E., Heath, R., Mayer, F.V., Carmena, D., Jing, C., Walker, P.A., Eccleston, J.F., Haire, L.F., et al. (2011). Structure of mammalian AMPK and its regulation by ADP. Nature 472:230-233. 10.1038/nature09932.
- Xing, H.L., Dong, L., Wang, Z.P., Zhang, H.Y., Han, C.Y., Liu, B., Wang, X.C., and Chen, Q.J. (2014). A CRISPR/Cas9 toolkit for multiplex genome editing in plants. BMC Plant Biol 14:327. 10.1186/s12870-014-0327-y.
- Yang, C., Ma, Y., He, Y., Tian, Z., and Li, J. (2018). OsOFP19 modulates plant architecture by integrating the cell division pattern and brassinosteroid signaling. Plant J 93:489-501. 10.1111/tpj.13793.
- Yang, C., Shen, W., Yang, L., Sun, Y., Li, X., Lai, M., Wei, J., Wang, C., Xu, Y., Li, F., et al. (2020). HY5-HDA9 Module Transcriptionally Regulates Plant Autophagy in Response to Light-to-Dark Conversion and Nitrogen Starvation. Mol Plant 13:515-531. 10.1016/j.molp.2020.02.011.
- Yang, F., Kimberlin, A.N., Elowsky, C.G., Liu, Y., Gonzalez-Solis, A., Cahoon, E.B., and Alfano, J.R. (2019). A Plant Immune Receptor Degraded by Selective Autophagy. Mol Plant 12:113-123. 10.1016/j.molp.2018.11.011.
- Yoshimoto, K., Hanaoka, H., Sato, S., Kato, T., Tabata, S., Noda, T., and Ohsumi, Y. (2004). Processing of ATG8s, ubiquitin-like proteins, and their deconjugation by ATG4s are essential for plant autophagy. Plant Cell 16:2967-2983. 10.1105/tpc.104.025395.
- **Zhai, Z., Keereetaweep, J., Liu, H., Feil, R., Lunn, J.E., and Shanklin, J.** (2018). Trehalose 6-Phosphate Positively Regulates Fatty Acid Synthesis by Stabilizing WRINKLED1. Plant Cell **30**:2616-2627. 10.1105/tpc.18.00521.
- Zhan, N., Wang, C., Chen, L., Yang, H., Feng, J., Gong, X., Ren, B., Wu, R., Mu, J., Li, Y., et al. (2018). S-Nitrosylation Targets GSNO Reductase for Selective Autophagy during Hypoxia Responses in Plants. Mol Cell **71**:142-154 e146. 10.1016/j.molcel.2018.05.024.
- **Zhang, X., Henriques, R., Lin, S.S., Niu, Q.W., and Chua, N.H.** (2006). Agrobacterium-mediated transformation of Arabidopsis thaliana using the floral dip method. Nat Protoc **1**:641-646. 10.1038/nprot.2006.97.

Zhang, X., Ding, X., Marshall, R.S., Paez-Valencia, J., Lacey, P., Vierstra, R.D., and Otegui, M.S. (2020). Reticulon proteins modulate autophagy of the endoplasmic reticulum in maize endosperm. Elife 910.7554/eLife.51918.

Zhou, J., Wang, Z., Wang, X., Li, X., Zhang, Z., Fan, B., Zhu, C., and Chen, Z. (2018). Dicot-specific ATG8-interacting ATI3 proteins interact with conserved UBAC2 proteins and play critical roles in plant stress responses. Autophagy **14**:487-504. 10.1080/15548627.2017.1422856.

Figures and Figure Legends

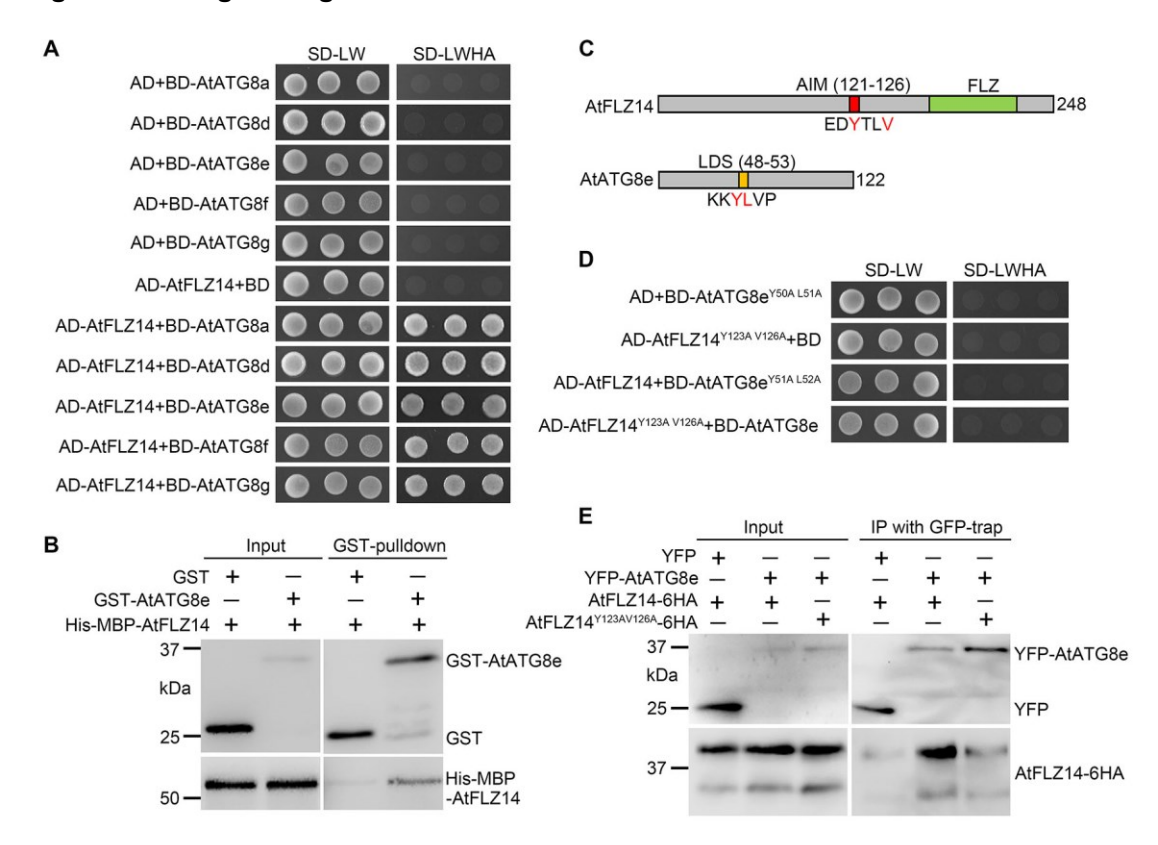


Figure 1. AtFLZ14 interacts with AtATG8s.

- (A) Y2H assays for the interaction between five representative AtATG8 isoforms and AtFLZ14. Protein interaction was determined by growth of the yeast cells co-transformed with various combinations of the plasmids on synthetic dropout medium lacking Leu and Trp (SD-LW) and synthetic dropout medium lacking Leu, Trp, His, and Ade (SD-LWHA). The three dots mean that three different colonies were picked for the interaction assay.
- (B) GST-pulldown assay showing the direct binding between AtATG8e and AtFLZ14 *in vitro*. Equal amount His-MBP-AtFLZ14 were incubated with GST or GST-AtATG8e bound to glutathione agarose beads, followed by protein elution and immunodetection with Anti-GST and anti-His antibodies.
- (C) Schematic representation of AtFLZ14 containing putative ATG8 interacting motif (AIM) and AtATG8e containing LIR-docking site (LDS). The amino acid position and residues corresponding to AIM or LDS are indicated above and below, respectively.
- (D) Y2H assays for the interaction between LSD-mutated AtATG8e (AtATG8eY50AL51A) and AIM-mutated AtFLZ14 (AtFLZ14Y123AV126A). Protein interaction was determined by growth of the yeast cells co-transformed with various combinations of the plasmids on synthetic dropout medium lacking Leu and Trp (SD-LW) and synthetic dropout medium lacking Leu, Trp, His, and Ade (SD-LWHA).

(E) Co-immunoprecipitation experiments revealing protein association between AtATG8e and AtFLZ15 *in vivo*. YFP or YFP-AtATG8e were transiently co-expressed in Arabidopsis protoplasts with AtFLZ14-6HA or AtFLZ14^{Y123AV126A}-6HA as indicated, and co-immunoprecipitation experiments were carried out using GFP-Trap. The protein elution was analyzed by immunoblotting using Anti-GFP and anti-HA antibodies.

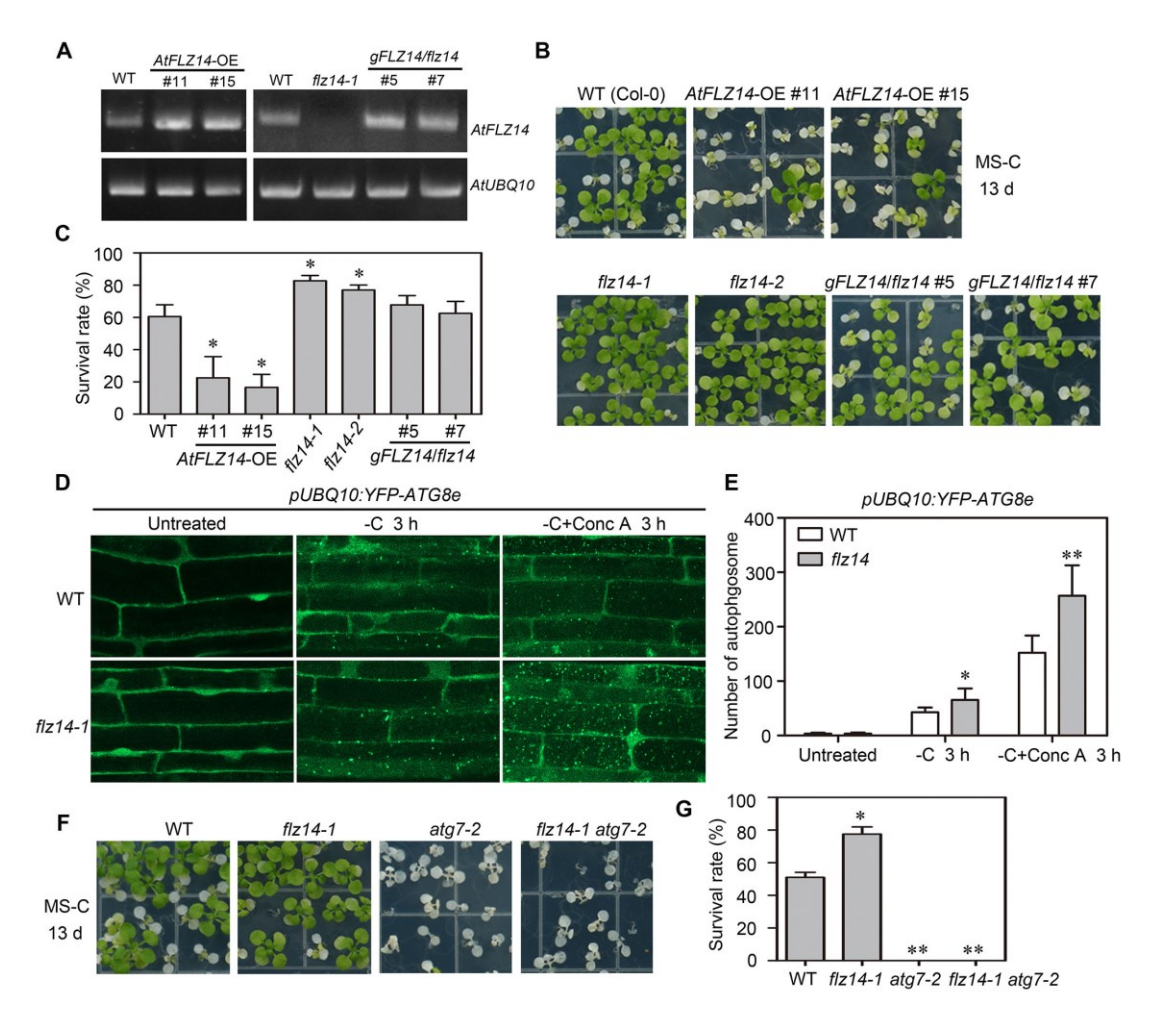


Figure 2. AtFLZ14 negatively regulates plant tolerance to carbon starvation.

- (A) Semiqutitative reverse transcription PCR analysis showing the gene expression of *AtFLZ14*. Total RNA was extracted from 7-day-old indicated seedlings (twenty seedlings for each batch) grown on MS medium plates under LD conditions. *AtUBQ10* was used as the internal control.
- (B) Photographs of seedlings with indicated genotypes subjected to fixed-carbon starvation treatment. Seedlings were grown on MS-C medium plates for 14 d under LD conditions, then subjected to darkness for 13 d, and then transferred back to LD conditions for recovery growth for another 7 d before imaging.
- (C) Statistic data for the survival rate showing in (B). Data are means \pm SD from three biological repeats. Statistical differences were calculated by a student's t test. The asterisk indicates statistically significant differences (* P < 0.05, **P < 0.01).
- (D) Confocal images of YFP-ATG8e-decorated autophagic vesicles in root cells. Five-day-old pUBQ10:YFP-ATG8e seedlings grown on MS medium plates under LD conditions were transferred to liquid MS-C medium supplemented with or without 1 μ M Conc A and incubated in darkness for 0 h and 3 h, followed by confocal observation of the root elongation zones. About 10 seedlings were observed with similar results.

- (E) Quantitative data of the number of autophagosome per frame showing in (D). Values are means \pm SD from 10 images from individual roots. Statistical differences were calculated by a student's t test. The asterisk indicates statistically significant differences (* P < 0.05, **P < 0.01).
- (F) Pictures of the WT, *flz14*, *atg7-2* and *flz14 atg7-2* seedlings subjected to fixed-carbon starvation treatment. Seedlings were grown on MS-C medium plates for 14 d under LD conditions, then subjected to darkness for 10 d, and then transferred back to LD conditions for recovery growth for another 7 d before being taken pictures.
- (G) Statistic data for the survival rate showing in (F). Data are means \pm SD from three biological repeats. Statistical differences were calculated by a student's t test. The asterisk indicates statistically significant differences (* P < 0.05, **P < 0.01).

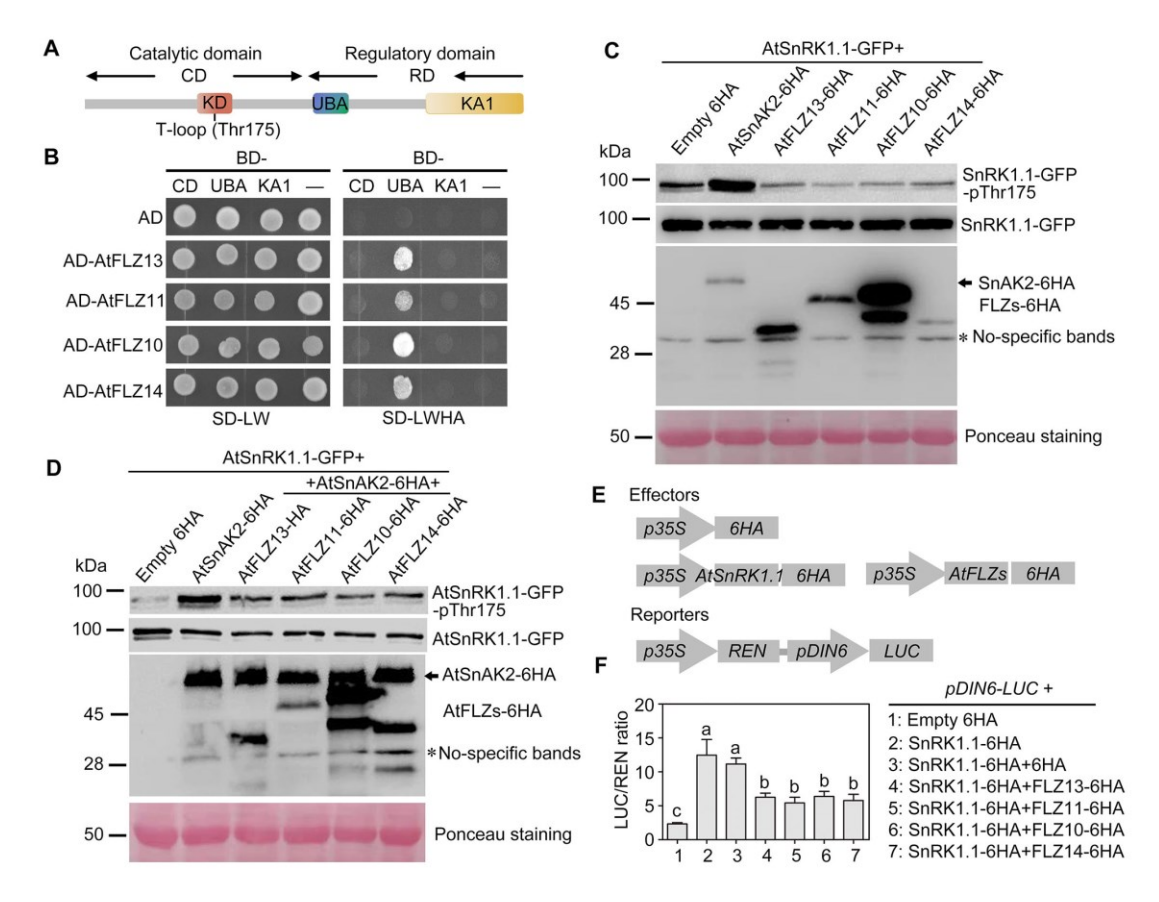


Figure 3. AtFLZs interact with and repress the activity of SnRK1.

- (A) Domain structure and function of AtSnRK1.1 protein.
- (B) Y2H assays for the interaction between AtFLZs with the different domain of AtSnRK1.1. Protein interaction was determined by growth of the yeast cells co-transformed with various combinations of the plasmids on synthetic dropout medium lacking Leu and Trp (SD-LW) and synthetic dropout medium lacking Leu, Trp, His, and Ade (SD-LWHA).
- (C) The effects of AtSnAK2 and AtFLZs on the protein accumulation and phosphorylation modification of AtSnRK1.1. AtSnRK1.1-GFP were transiently co-expressed in *N. Benthamian* with either AtSnAK2-6HA or individual AtFLZs-6HA fusion, and the total proteins were extracted 3 d after Agrobacterium infiltration for immunoblotting using Anti-AMPKT¹⁷⁵, Anti-GFP and anti-HA antibodies. Ponceau staining denotes protein loading.
- (D) The effect of AtFLZs on AtSnAK2-induced phosphorylation of AtSnRK1.1. AtSnRK1.1-GFP were transiently co-expressed in *N. Benthamian* with AtSnAK2-6HA and AtFLZs-6HA as indicated, and the total proteins were extracted 3 d after Agrobacterium infiltration for immunoblotting using Anti-AMPKT¹⁷⁵, Anti-GFP and anti-HA antibodies. Ponceau staining denotes protein loading.
- (E) Schematic of the effectors and reporters used in the dual-luciferase reporter assays.

(F) Transient dual-luciferase reporter assays showing the activity of DIN6 promoter (activation) in Arabidopsis protoplasts upon transient co-expression of AtSnRK1.1 with 6HA or AtFLZs-6HA. Values are means \pm SD from four biological replicates. Different letters above the bars indicate significant differences (P < 0.05) obtained by one-way analysis of variance (ANOVA).

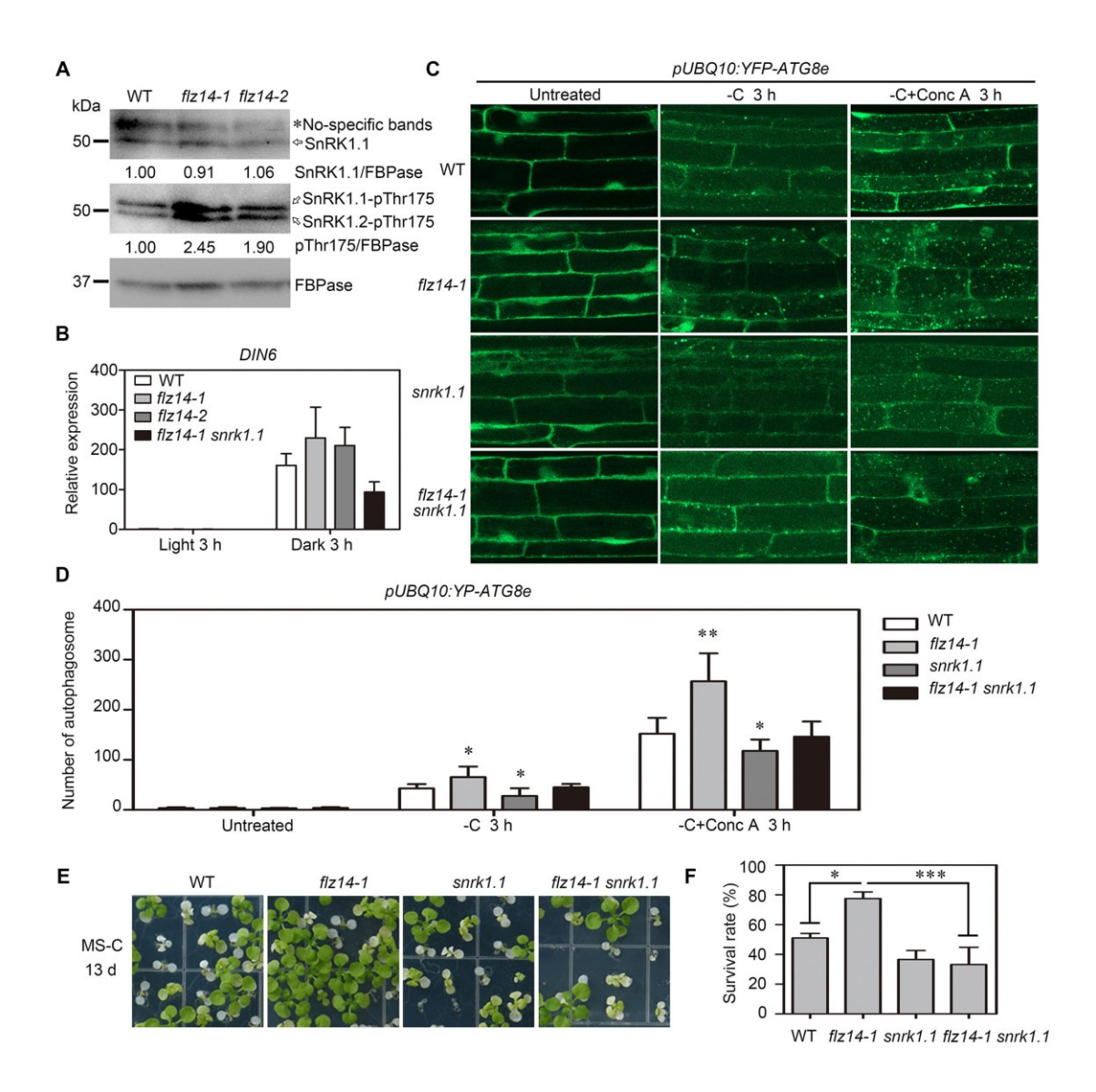


Figure 4. Genetic interaction between AtFLZ14 and AtSnRK1.1 in the regulation of autophagy and plant tolerance in response to carbon starvation.

- (A) The level of total AtSnRK1.1 and phosphorylated AtSnRK1.1 (Thr175) in the WT and *flz14* mutants. Seven-day-old seedlings grown on MS medium plates under LD conditions were transferred to MS-C liquid medium and subjected to dark treatment for 3 h before being harvested to extract total proteins for immunoblotting using Anti-SnRK1.1, Anti-AMPKT¹⁷⁵, Anti-GFP and anti-FBPase antibodies. The number blow the gels are the relative ratio of SnRK1.1 or SnRK1-T175 to FBPase.
- (B) Quantitative real-time PCR assay showing the expression of DIN6 in the indicated plants treated under control (light 3 h) or energy stress (dark 3 h) conditions. Total RNA was extracted from six the 5th leaves of three-week-old indicated plants grown in soil under LD conditions with or without dark exposure for 3 h. The treatment was always initiated 3 h after the onset of the light period. AtUBQ10 was used as the internal control. Data are means \pm SD (n = 9 from three biological repeats, each biological repeat with

three technical repeats). Statistical differences were calculated by a student's t test. The asterisk indicates statistically significant differences (**P < 0.01).

- (C) Confocal images of YFP-ATG8e-decorated autophagic vesicles in root cells. Five-day-old seedlings grown on MS medium plates under LD conditions were transferred to liquid MS-C medium supplemented with or without 1 μ M Conc A and incubated in darkness for 0 h and 3 h, followed by confocal observation of root cells at the elongation zones. About 10 seedlings were observed with similar results.
- (D) Quantitative data of the number of autophagosome per frame showing in (C). Values are means \pm SD from 10 images captured from individual roots. Statistical differences were calculated by a student's t test. The asterisk indicates statistically significant differences (*P < 0.05, **P < 0.01).
- (E) Pictures of the WT, *flz14-1*, *snrk1.1* and *flz14-1 snrk1.1* seedlings subjected to fixed-carbon starvation treatment. Seedlings were grown on MS-C medium plates for 14 d under LD conditions, then subjected to darkness for 13 d, and then transferred back to LD conditions for recovery growth for another 7 d before being taken pictures.
- (F) Statistic data for the survival rate showing in (E). Data are means \pm SD from three biological repeats. Statistical differences were calculated by a student's t test. The asterisk indicates statistically significant differences (*P < 0.05, **P < 0.01).

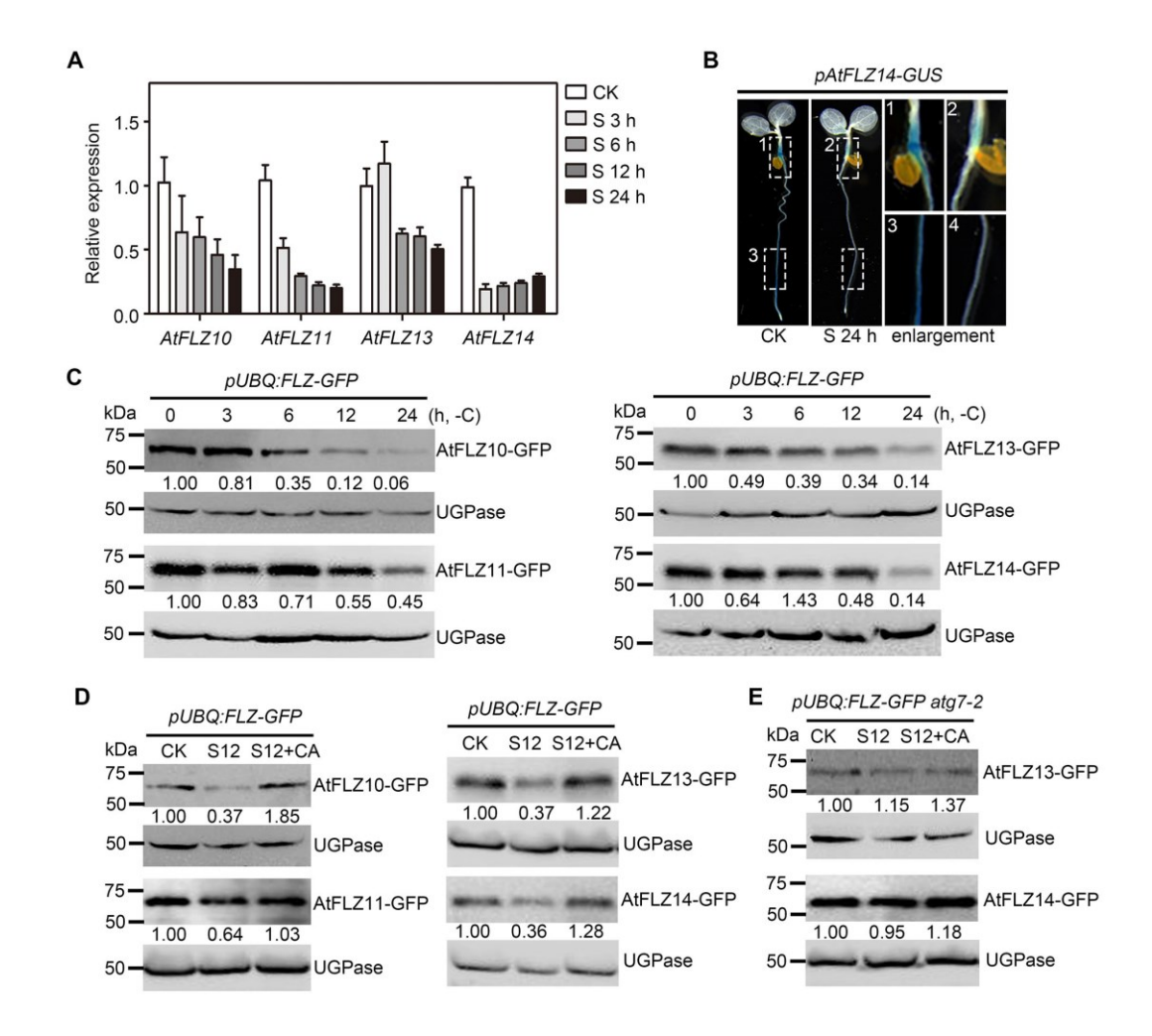


Figure 5. Carbon starvation represses *AtFLZ* gene expression and promotes the autophagic degradation of AtFLZ proteins.

- (A) Quantitative real-time PCR assay showing the expression of AtFLZ10/11/13/14 in response to carbon starvation. Five-day-old WT seedlings grown on MS medium plates under LD conditions were exposed to continuous light for 1 d before being subjected to MS-C medium and kept in darkness for 0, 3, 6, 12 and 24 h (marked as S 0h, S 3h, S 6h, S 12h and S 24 h, respectively). Total RNA was extracted from three different batches (20 seedlings for each batch) with the indicated treatment. AtUBQ10 was used as the internal control. Data are means \pm SD (n = 6 from three biological repeats, each biological repeat with two technical repeats). Different letters above the bars indicate significant differences (P < 0.05) obtained by one-way analysis of variance (ANOVA).
- (B) GUS staining showing the repressive effect of carbon starvation to the expression of *AtFLZ14*. Five-day-old *pAtFLZ14-GUS* seedlings grown on MS medium plates under LD conditions were exposed to continuous light for 1 d before being subjected to MS-C medium in darkness for 24 h (S 24 h) or MS + 1% sucrose medium in light for 24 h (CK), followed by *GUS* staining and imaging.

- (C) Detection of protein levels of AtFLZ10/1113/14-GFP upon carbon starvation. Seven-day-old seedlings grown on MS medium plates under LD conditions were transferred to liquid MS-C medium and subjected to dark treatment for 0, 3, 6, 12 and 24 h, followed by protein extraction and immunodetection using Anti-GFP and anti-UGPase antibodies. The number blow the gels are the relative ratio of FLZ-GFP to UGPase.
- (D) Detection of protein levels of AtFLZ10/11/13/14-GFP upon carbon starvation and Conc A treatment. Seven-day-old seedlings grown on MS medium plates under LD conditions were transferred to liquid MS-C medium with or without 1 μ M Conc A and subjected to dark treatment for 12 h, followed by protein extraction and immunodetection using anti-GFP and anti-UGPase antibodies. The number blow the gels are the relative ratio of FLZ-GFP to UGPase.
- (E) Detection of protein levels of AtFLZ13/14-GFP in *atg7-2* background upon carbon starvation. Seven-day-old seedlings grown on MS medium plates under LD conditions were transferred to liquid MS-C medium and subjected to dark treatment for 12 h, , followed by protein extraction and immunodetection using anti-GFP and anti-UGPase antibodies. The number blow the gels are the relative ratio of FLZ-GFP to UGPase.

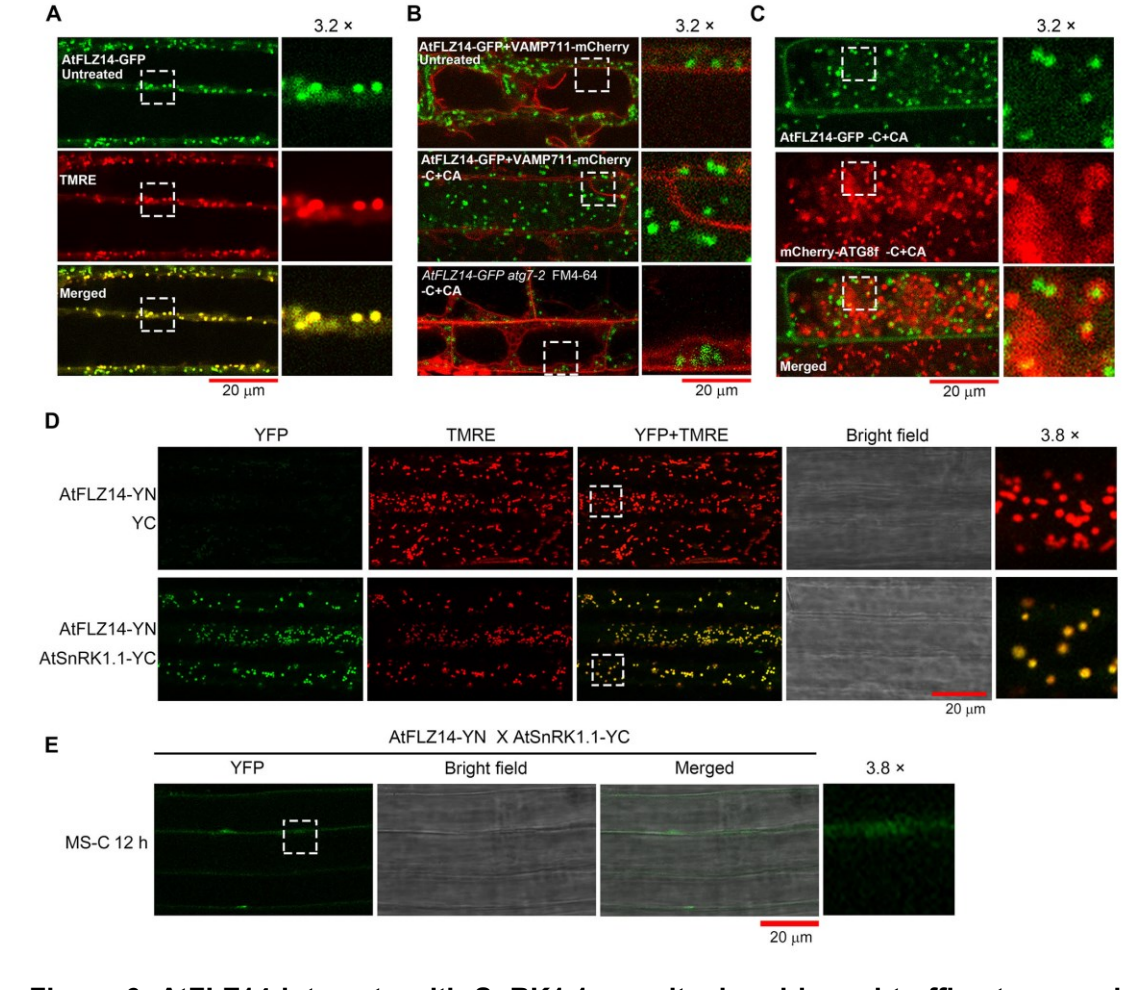


Figure 6. AtFLZ14 interacts with SnRK1.1 on mitochondria and traffics to vacuole upon carbon starvation.

- (A) Confocal images of AtFLZ14-GFP in Arabidopsis root cells. Five-day-old *pUBQ10:AtFLZ14-GFP* seedlings grown on MS medium plates under LD conditions were stained with the mitotracker TMRE for 5 min, followed by confocal observation.
- (B) Confocal micrographs of Arabidopsis root cells co-expressing AtFLZ14-GFP and the tonoplast marker mCherry-VAMP711. Upper panel: Five-day-old seedlings were grown on MS medium plates without treatment. Middle panel: the seedlings grown on MS medium plates were subjected to MS-C liquid medium containing 1 μ M Conc A for 12 h before being observed. Lower panel: Five-day-old *pUBQ10: AtFLZ14-GFP atg7-2* seedlings grown on MS medium plates under LD conditions were subjected to MS-C liquid medium containing 5 μ M FM4-64 for 6 h, then were incubated with 1 μ M Conc A for another 12 h in darkness, followed by confocal observation.
- (C) Confocal micrographs of Arabidopsis root cells co-expressing AtFLZ14-GFP and the autophagosome marker mCherry-ATG8f. Five-day-old seedlings grown on MS medium plates were subjected to MS-C liquid medium containing 1 μM Conc A for 12 h before confocal observation.

- (D) Confocal micrographs of Arabidopsis root cells expressing a AtFLZ14-YN with empty YC and AtSnRK1.1-YC, respectively. Five-day-old seedlings grown on MS medium plates under LD conditions were stained with the mitotracker TMRE for 5 min, followed by confocal observation.
- (E) Confocal micrographs showing the effect of carbon starvation on the AtFLZ14-AtSnRK1.1 interaction. Five-day-old seedlings grown on MS medium plates under LD conditions were subjected to MS-C liquid medium for 12 h in darkness followed by confocal observation.

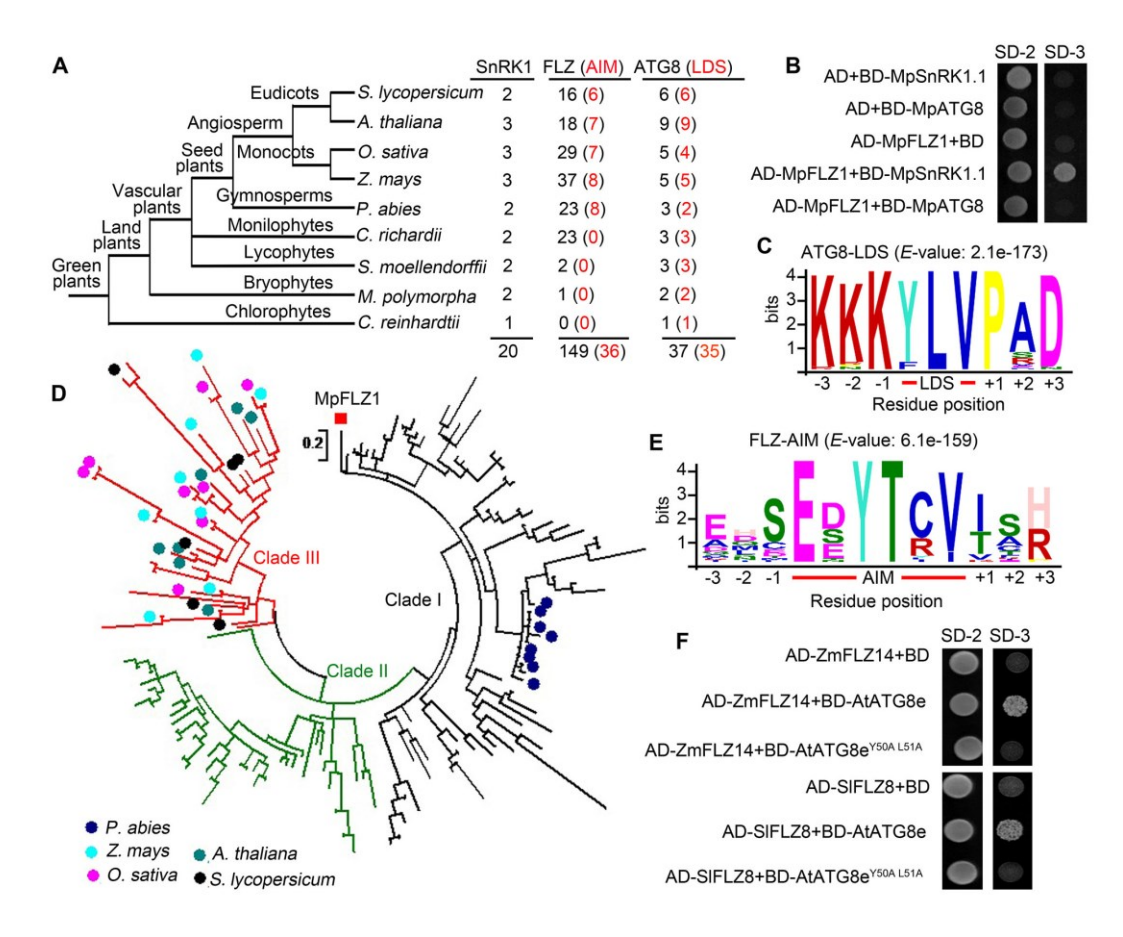


Figure 7. Evolutionary conservation of SnRK1-FLZ-ATG8 module.

- (A) simplified cladogram of the species selected for screening putative SnRK1, FLZ and ATG8 proteins. Figures in the right column indicate the total numbers of them found in each species.
- (B) Y2H assays for the interaction between FLZ with ATG8 and SnRK1 from liverwort. Protein interaction was determined by growth of the yeast cells co-transformed with various combinations of the plasmids on synthetic dropout medium lacking Leu and Trp (SD-LW) and synthetic dropout medium lacking Leu, Trp and His (SD-LWH).
- (C) Phylogenetic analysis of 149 plant FLZ proteins from 8 plant genomes as shown in (A). The phylogenetic tree was constructed based on the multiple sequence alignments of FLZ proteins and generated with MEGA 5.0 software using the Maximum Likelihood method. The evolutionary distances were computed using the JTT matrix-based method.
- (D) The consensus ATG8-LDS sequence identified by MEME using the 35 screened LSD sequence as shown in (A).
- (E) The consensus FLZ-AIM sequence identified by MEME using the 36 AIM sequence as shown in (A).
- (F) Y2H assays for the interaction between AtATG8e with ZmFLZ14 and SIFLZ14. Protein interaction was determined by growth of the yeast cells co-transformed with various

combinations of the plasmids on synthetic dropout medium lacking Leu and Trp (SD-LW) and synthetic dropout medium lacking Leu, Trp, and His (SD-LWH).

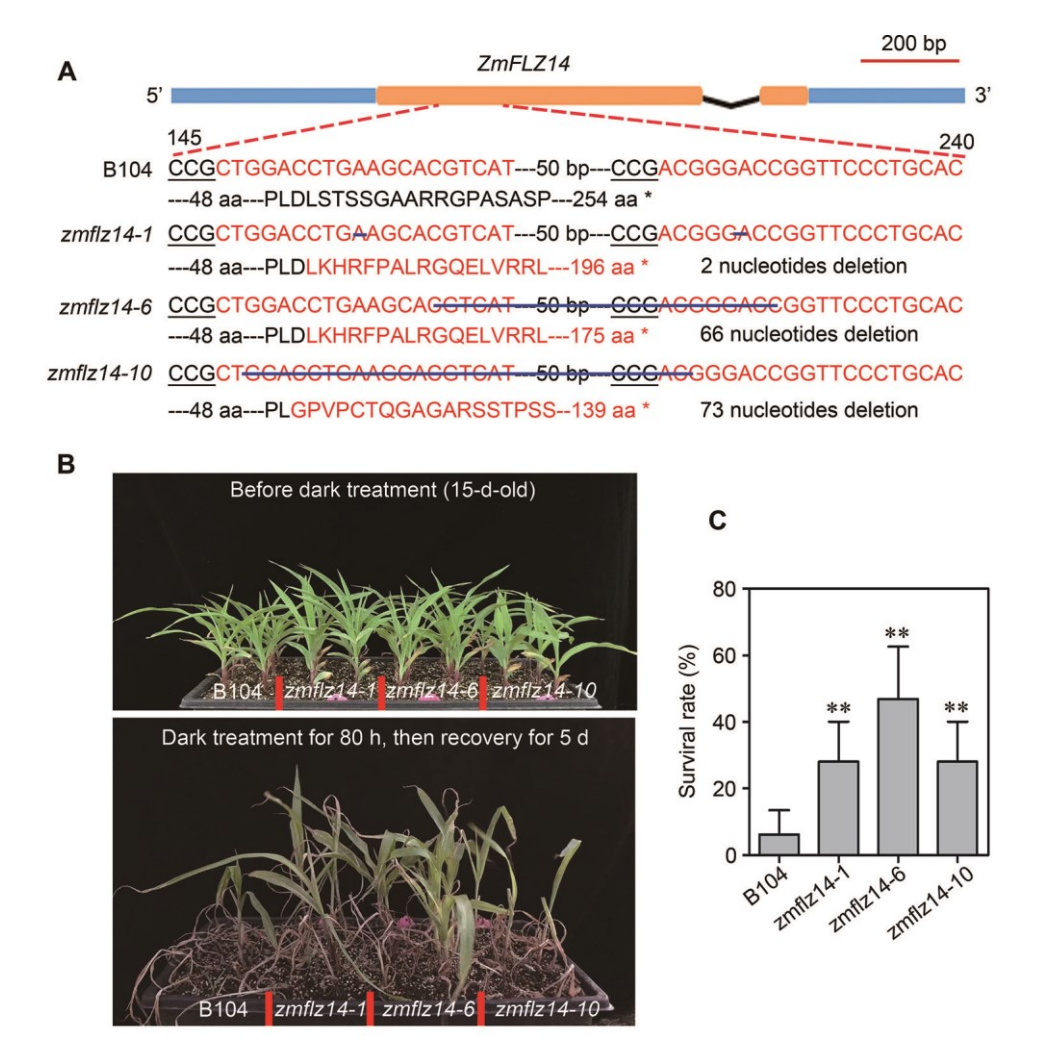


Figure 8. Knockout of *ZmFLZ14* confers tolerance of maize to long-term dark treatment.

- (A) Schematic illustrations of *zmflz14* Crispr/CAS9 gene editing lines. The guide RNA target sequence is shown and protospacer adjacent motif sequences are underlined. Sequencing result of the isolated mutant allele and predicted mutant protein sequences of ZmFLZ14 are shown.
- (B) Pictures of the WT (B104) and three Crispr/CAS9 lines subjected to dark treatment. Seedlings were grown in soil for 15 d under LD conditions, then subjected to darkness for 80 h, and then transferred back to LD conditions for recovery growth for another 5 d before being taken pictures.
- (C) Statistic data for survival rate showing in (B). Data are means \pm SD from four biological repeats. Statistical differences were calculated by a student's t test. The asterisk indicates statistically significant differences (**P < 0.01).

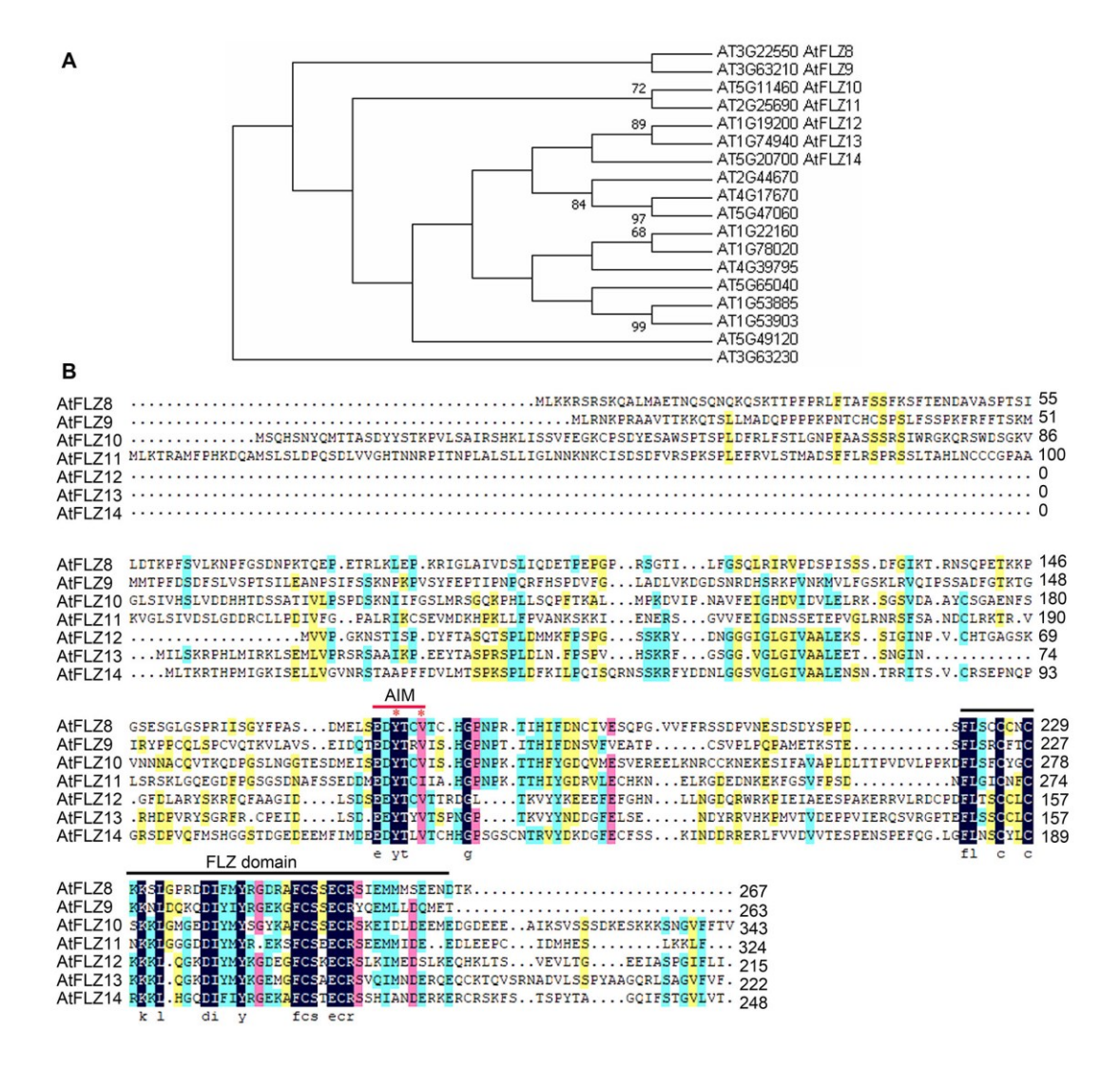


Figure S1. Phylogenetic and protein sequence alignment of AtFLZ proteins.

- (A) Phylogenetic relationships of FLZ proteins from Arabidopsis. The phylogenetic tree was constructed based on the multiple sequence alignments of FLZ proteins and generated with MEGA 5.0 software using the Neighbor-Joining method.
- (B) Amino acid sequence alignment of the seven AIM-containing FLZ proteins. The conserved FLZ domain and AIM is highlighted and marked with lines.

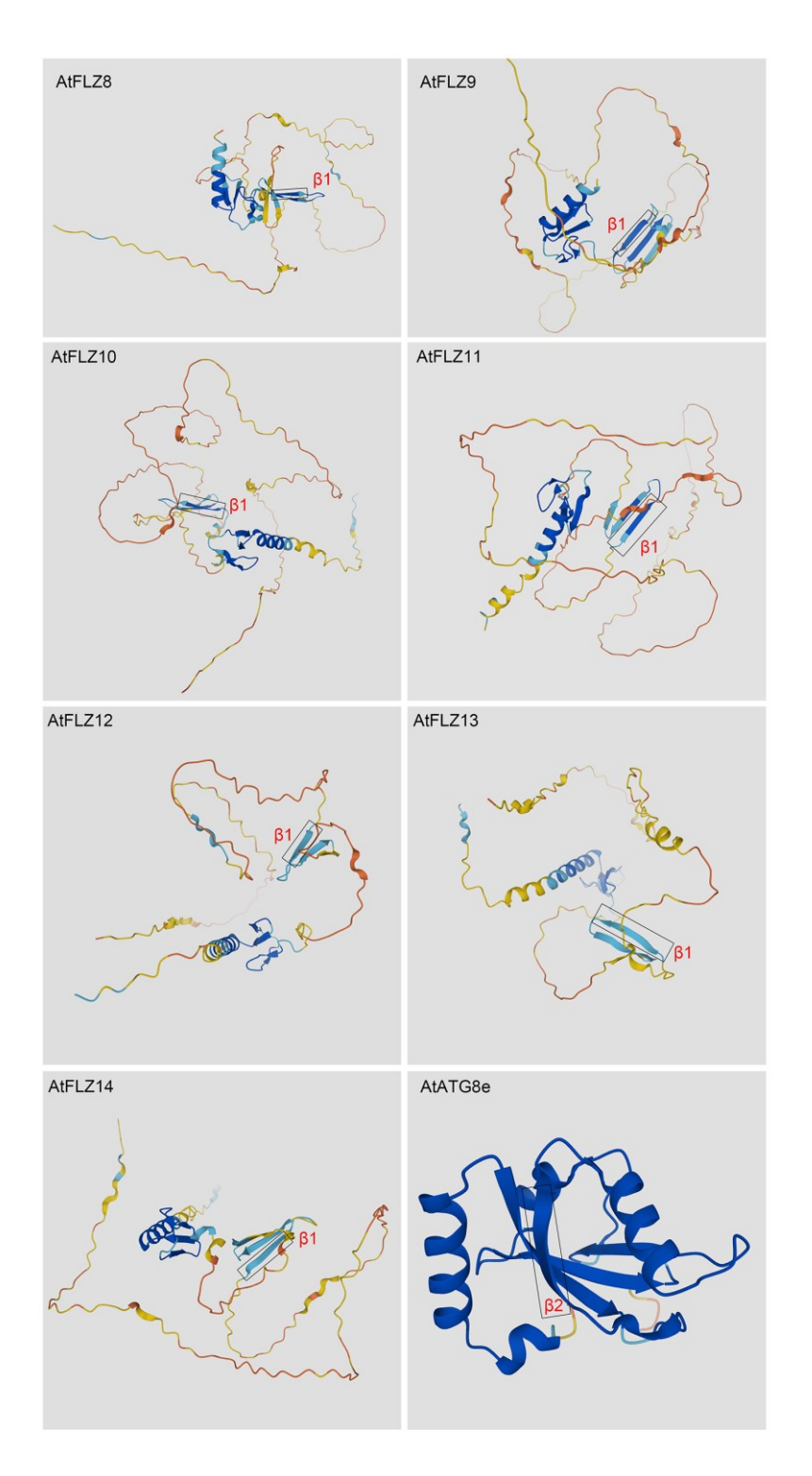


Figure S2. Predicted protein structure of AtFLZ and ATG8e by AlphaFold.

The protein structure of the seven AtFLZs and AtATG8e, and the box marked the position of AIM or LDS, respectively. The data were retrieved from https://alphafold.ebi.ac.uk/.

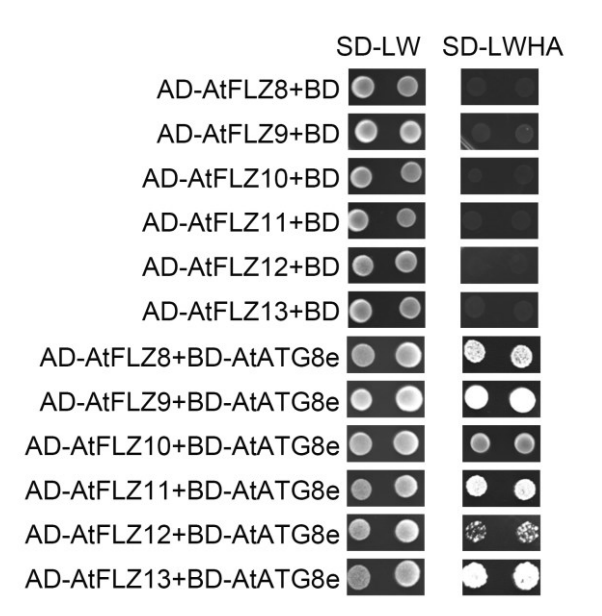


Figure S3. The interaction between AtATG8e with the six AlM-containing AtFLZs by **Y2H assays.** Protein interaction was determined by growth of the yeast cells co-transformed with various combinations of the plasmids on synthetic dropout medium lacking Leu and Trp (SD-LW) and synthetic dropout medium lacking Leu, Trp, His, and Ade (SD-LWHA).

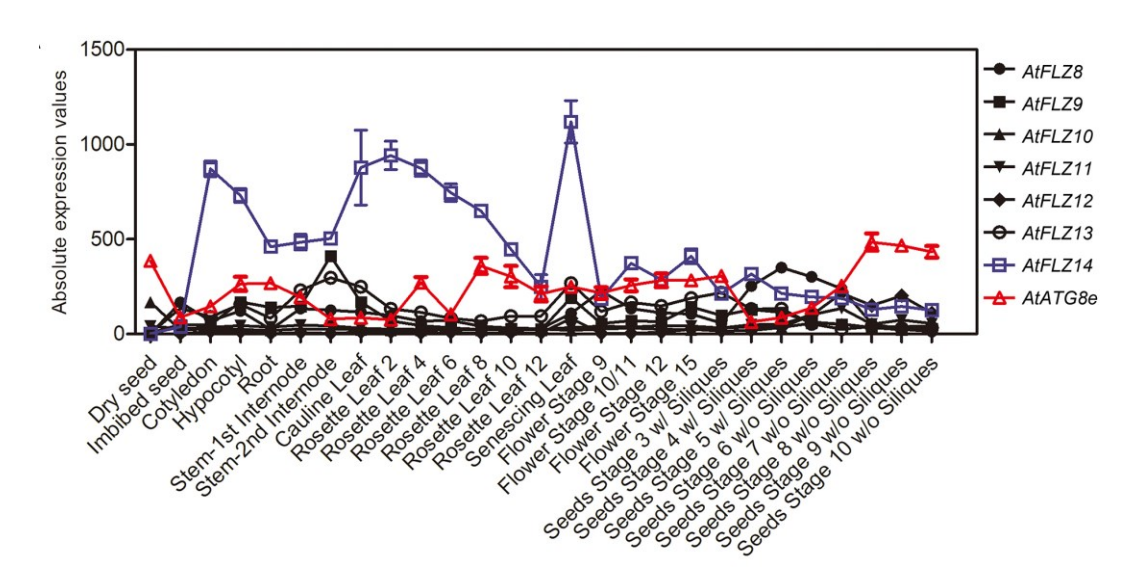


Figure S4. Expression profiles of *AtFLZs* and *AtATG8e* in different Arabidopsis tissues.

The absolute expression data of each gene were downloaded from the Arabidopsis e-FP browser: http://bbc.botany.utoronto.ca/efp/cgi-bin/efpWeb.cgi.

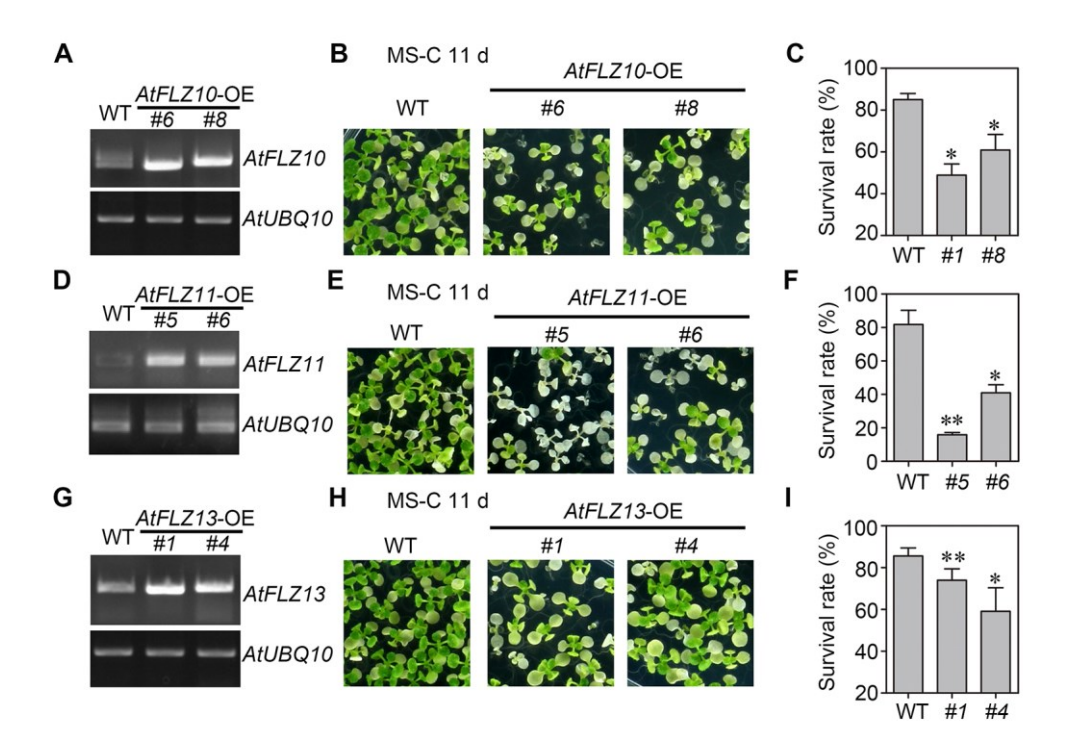


Figure S5. Overexpression of AtFLZ10/11/13 confers hypersensitivity of plants to carbon starvation.

- (A) Semi-quantitative reverse transcription PCR analysis showing the gene expression of *AtFLZ10*. Total RNA was extracted from 7-day-old indicated seedlings (twenty seedlings for each batch) grown on MS medium plates under LD conditions. *AtUBQ10* was used as the internal control.
- (B) Pictures of the WT and two independent *AtFLZ10* overexpressing lines subjected to dark treatment. Seedlings were grown on MS-C medium plates for 14 d under LD conditions, then subjected to darkness for 11 d, and then transferred back to LD conditions for recovery growth for another 7 d before being taken pictures.
- (C) Statistic data for the survival rate showing in (B). Data are means \pm SD from three biological repeats. Statistical differences were calculated by a student's t test. The asterisk indicates statistically significant differences (*P < 0.05).
- (D) Semi-quantitative reverse transcription PCR analysis showing the gene expression of *AtFLZ11*. Total RNA was extracted from 7-day-old indicated seedlings (twenty seedlings for each batch) grown on MS medium plates under LD conditions. *AtUBQ10* was used as the internal control.
- (E) Pictures of the WT and two independent *AtFLZ11* overexpressing lines subjected to dark treatment. Seedlings were grown on MS-C medium plates for 14 d under LD conditions, then subjected to darkness for 11 d, and then transferred back to LD conditions for recovery growth for another 7 d before being taken pictures.
- (F) Statistic data for the survival rate showing in (E). Data are means ± SD from three

biological repeats. Statistical differences were calculated by a student's t test. The asterisk indicates statistically significant differences (*P < 0.05, **P < 0.01).

- (G) Semi-quantitative reverse transcription PCR analysis showing the gene expression of *AtFLZ13*. Total RNA was extracted from 7-day-old indicated seedlings (twenty seedlings for each batch) grown on MS medium plates under LD conditions. *AtUBQ10* was used as the internal control.
- (H) Pictures of the WT and two independent *AtFLZ13* overexpressing lines subjected to dark treatment. Seedlings were grown on MS-C medium plates for 14 d under LD conditions, then subjected to darkness for 11 d, and then transferred back to LD conditions for recovery growth for another 7 d before being taken pictures.
- (I) Statistic data for the survival rate showing in (H). Data are means \pm SD from three biological repeats. Statistical differences were calculated by a student's t test. The asterisk indicates statistically significant differences (*P < 0.05, **P < 0.01).

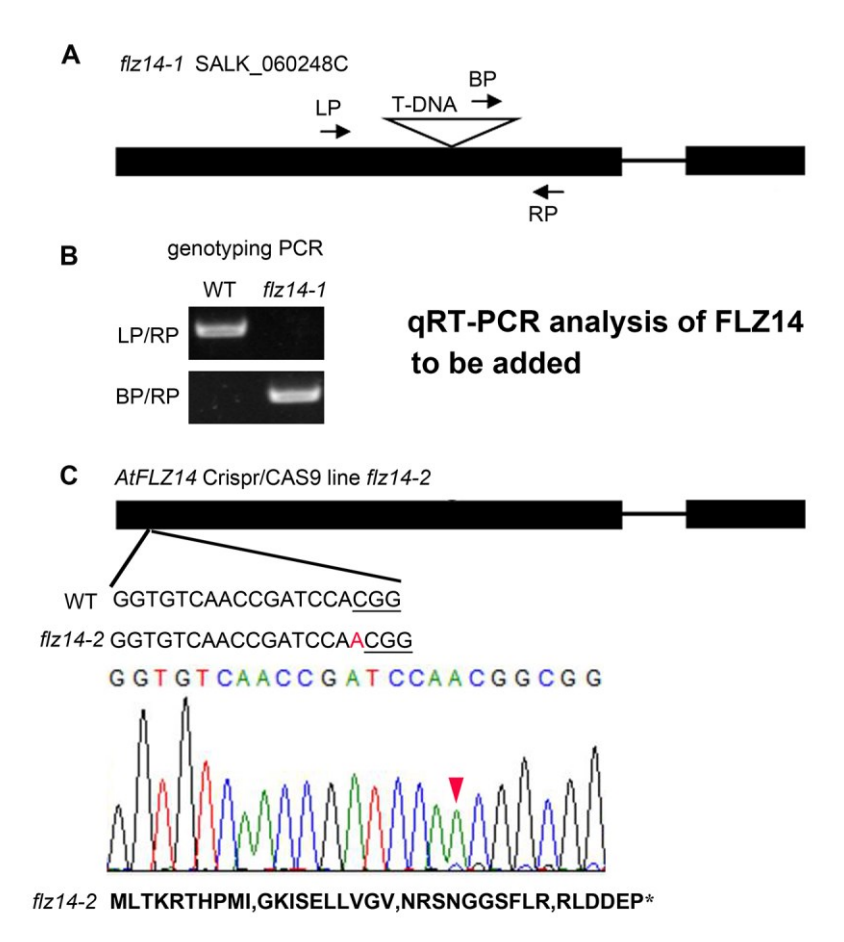


Figure S6. Molecular identification of the flz14 mutants.

- (A) The gene structure of *AtFLZ14* and the corresponding T-DNA insertion mutant used in this study. Black bars indicate exons and lines introns.
- (B) Genotyping of the *flz14-1* T-DNA insertion mutant. A three-primer PCR assay was used to identify the homozygous *flz14-1* mutant. BP, border primer; LP, left primer; RP, right primer, as shown in (A).
- (C) Schematic illustrations of *Atflz14-2* Crispr/CAS9 gene editing line. Black bars indicate exons and lines introns. The guide RNA target sequence is shown and protospacer adjacent motif sequences are underlined. Sequencing result of the isolated mutant allele and predicted mutant protein sequences of AtFLZ14 are shown. Arrowheads indicate the site of mutation.

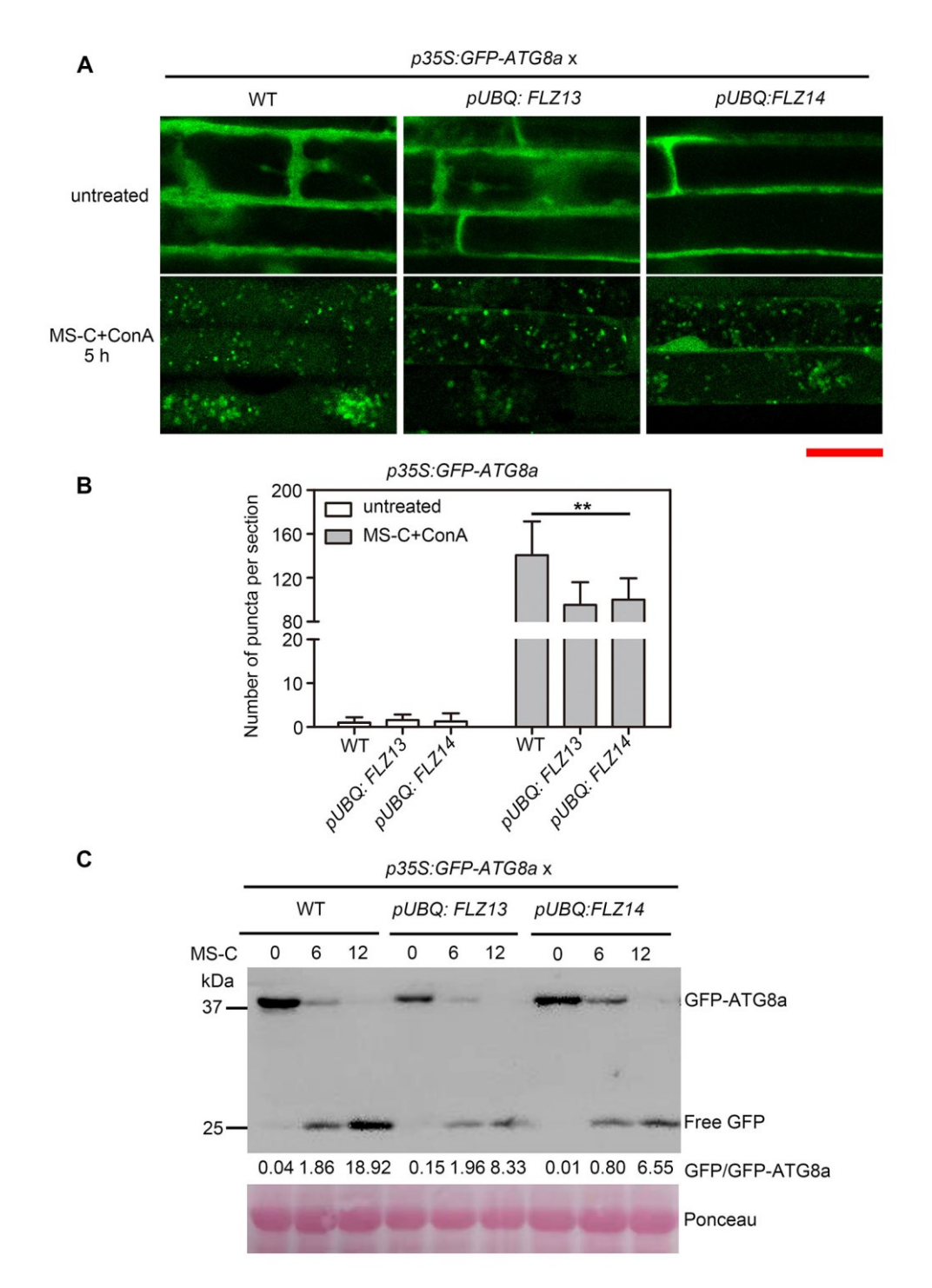


Figure S7. Overexpression of AtFLZ13/14 decrease the activity of autophagy upon carbon starvation treatment.

- (A) Confocal images of YFP-ATG8e-decorated autophagic vesicles in root cells. Five-day-old seedlings grown on MS medium plates under LD conditions were transferred to liquid MS-C medium with or without containing 1 μ M Conc A and incubated in darkness for 0 h and 5 h, then the root cells at the elongation zones were imaged using a Zeiss LSM 800 confocal fluorescence microscopy. Five seedlings were observed with similar results.
- (B) Quantitative data of the number of autophagosome per frame showing in (A). Values

are means \pm SD from 10 frames. Statistical differences were calculated by a student's t test. The asterisk indicates statistically significant differences (**P < 0.01).

(C) GFP-ATG8a cleavage assay showing the autophagic activity of the indicated plants upon carbon starvation treatment. Five-day-old seedlings grown on MS medium plates under LD conditions were exposed to continuous light for 1 d before being subjected to MS-C medium and kept in darkness for 0, 6 and 12 h. Then the seedlings were harvested to isolate total proteins for Western blotting analysis using Anti-GFP antibodies. Ponceau staining denotes protein loading. The number blow the gels are the relative ratio of GFP-ATG8a to GFP.

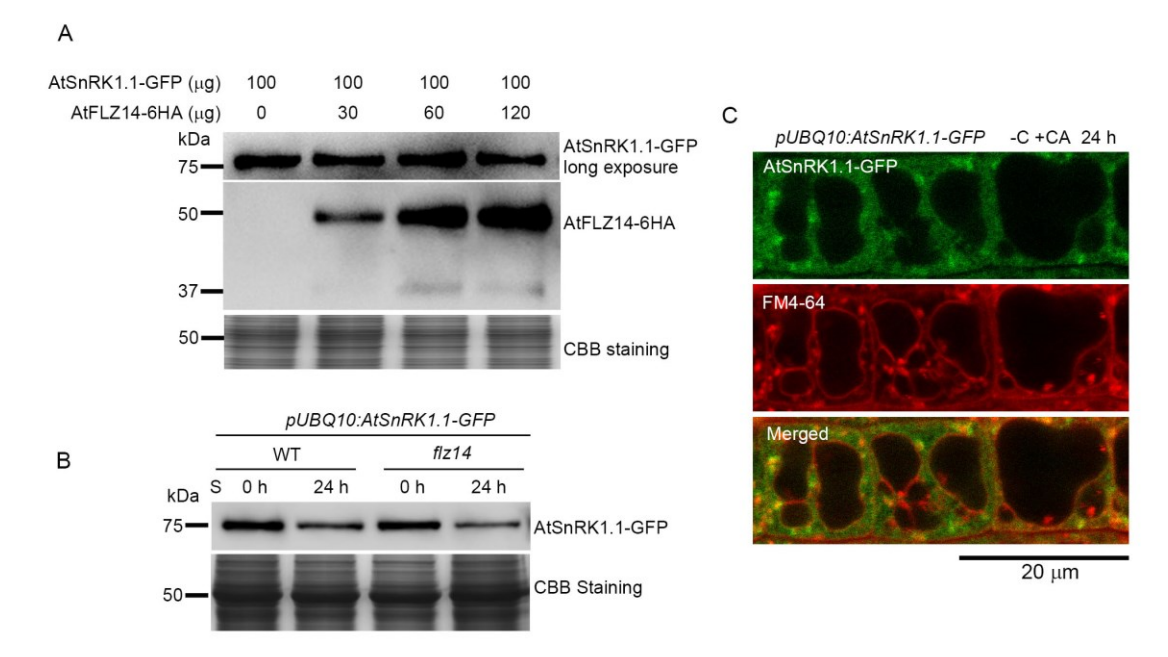


Figure S8. AtFLZ14 does not affect the protein accumulation of AtSnRK1.1.

- (A) The effect of AtFLZ14 on the protein accumulation of SnRK1.1. Equal amount AtSnRK1.1-YFP plasmid (100 μ g) were separately co-transfected with 0, 30, 60 and 120 μ g AtFLZ14-6HA plasmid into Arabidopsis suspension cells, then the transformed cells were incubated in darkness for 12 h before being harvested to extract total protein for immunoblotting using Anti-GFP and Anti-HA antibodies. CBB staining denotes the protein loading.
- (B) The level of AtSnRK1.1-GFP in WT and *flz14-1* backgrounds upon carbon starvation. Five-day-old seedlings grown on MS medium plates under LD conditions were immersed in MS-C liquid medium and kept in darkness for 0 or 24 h before being harvested to extract total protein for immunoblotting using Anti-GFP antibodies. Ponceau staining denotes the loading control.
- (C) Confocal images of SnRK1.1-GFP in Arabidopsis root cells upon carbon starvation. Five-day-old seedlings grown on MS medium plates under LD conditions were immersed in MS-C liquid medium containing 5 μ M FM4-64 for 6 h in darkness, then were incubated 1 μ M Conc A with for another 12 h before being imaged.

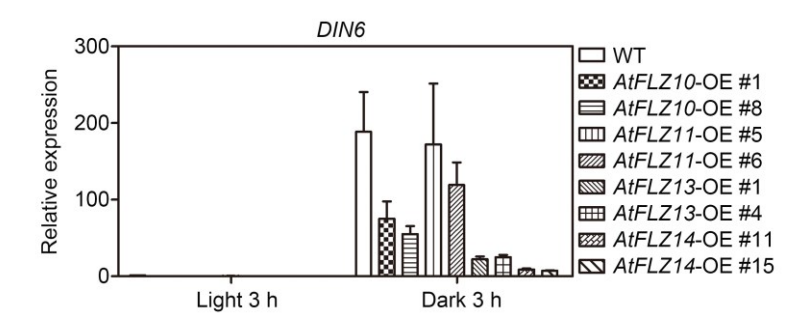


Figure S9. Expression analysis of DIN6 in AtFLZ overexpression lines.

Quantitative real-time PCR assay showing the expression of *DIN6* in the indicated plants treated under control (light 3 h) or energy stress (dark 3 h) conditions. Total RNA was extracted from 6 the 5th leaves of three-week-old indicated plants grown in soil under LD conditions with or without dark exposure for 3 h. The treatment was always initiated 3 h after the onset of the light period. *AtUBQ10* was used as the internal control. Data are means \pm SD (n = 9 from three biological repeats, each biological repeat with three technical repeats). Statistical differences were calculated by a student's t test. The asterisk indicates statistically significant differences (**P < 0.01).

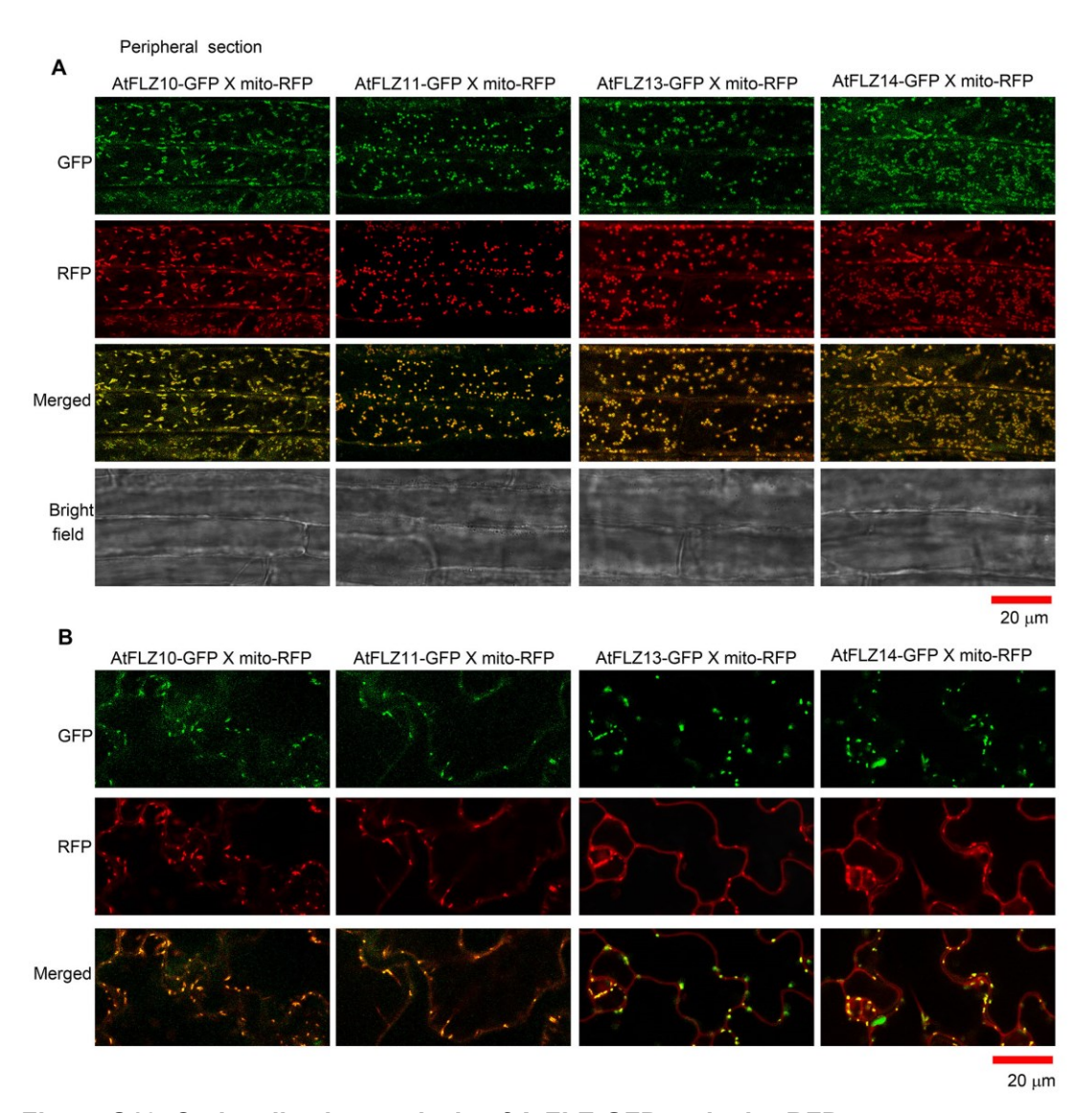


Figure S10. Co-localization analysis of AtFLZ-GFP and mito-RFP.

- (A) Confocal micrographs of Arabidopsis root cells expressing a AtFLZ-GFP and mito-RFP.
- (B) Confocal micrographs of Arabidopsis leaf epidermal cells expressing a AtFLZ-GFP and mito-RFP.

Five-day-old seedlings grown on MS medium plates under LD conditions were used to observe the co-localization using a Zeiss LSM 880 confocal fluorescence microscopy.

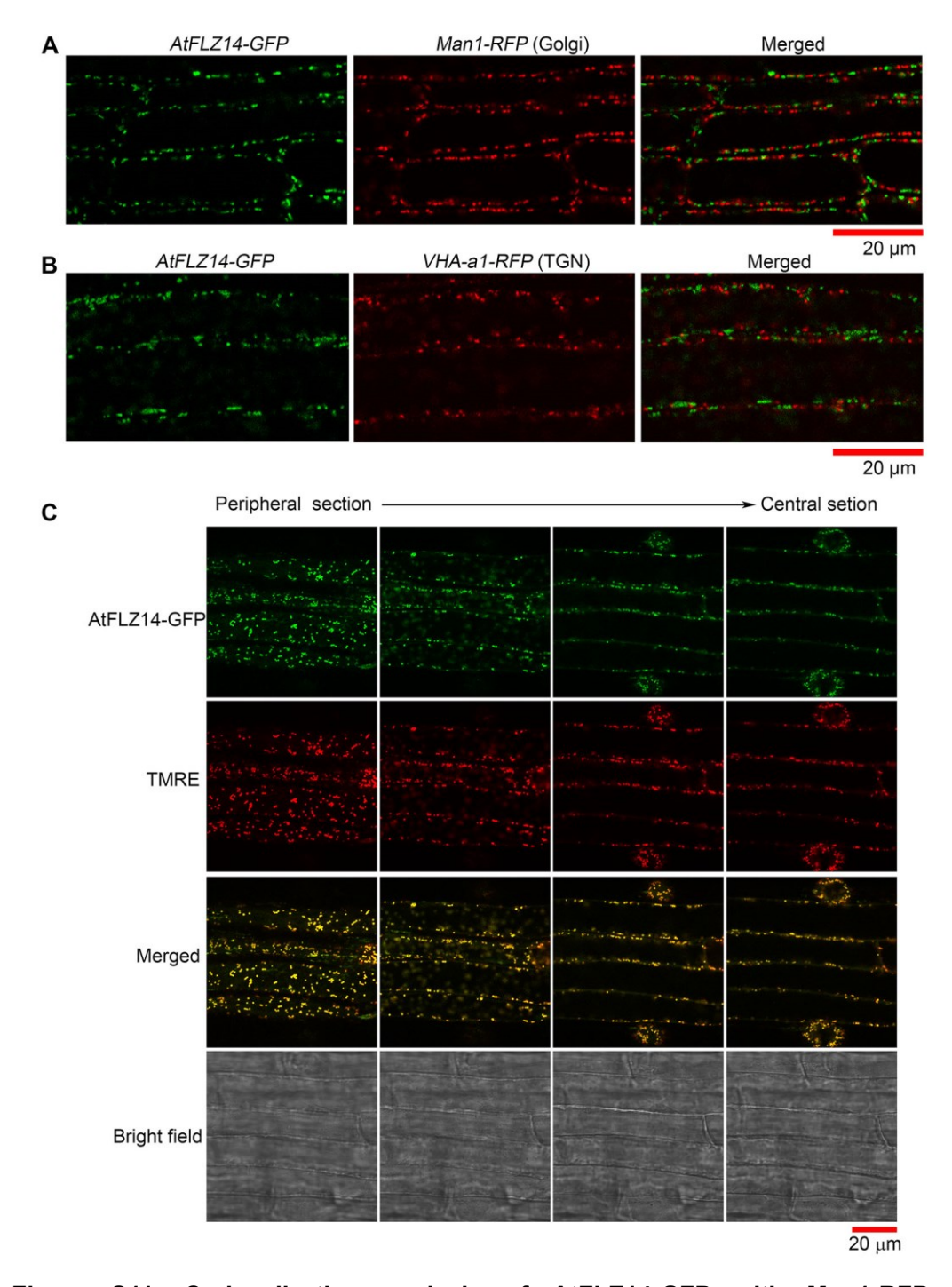


Figure S11. Co-localization analysis of AtFLZ14-GFP with Man1-RFP and VHA-a1-RFP.

- (A) Confocal micrographs of Arabidopsis root cells co-expressing AtFLZ14-GFP and the Golgi marker Man1-RFP.
- (B) Confocal micrographs of Arabidopsis root cells co-expressing AtFLZ14-GFP and the TGN marker VHA-a1-RFP.
- (C) Localization of AtFLZ14-GFP to mitochondria as stained by mito-tracker TMRE. Five-day-old seedlings grown on MS medium plates under LD conditions were used to observe the co-localization using a Zeiss LSM 880 confocal fluorescence microscopy.

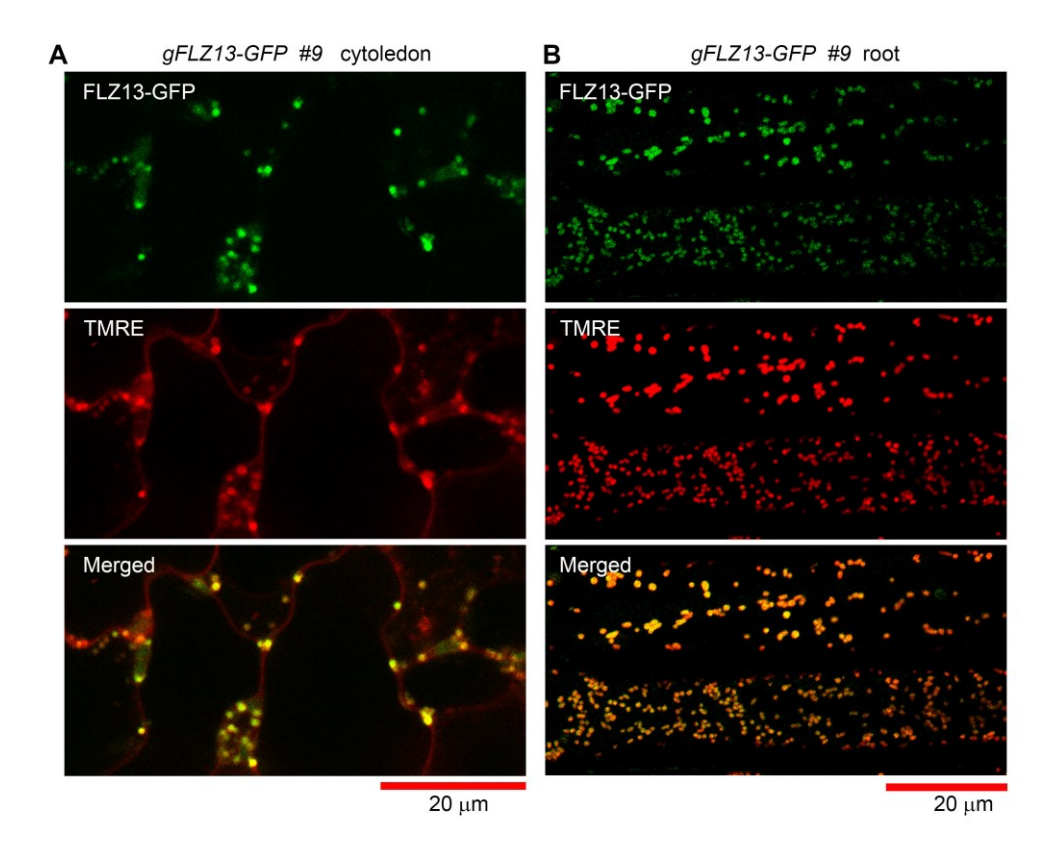


Figure S12. Subcellular localization analysis of AtFLZ13-GFP.

Confocal micrographs of Arabidopsis cotyledon epidermal cells (A) or root cells (B) expressing *gAtFLZ13-GFP*. Five-day-old seedlings grown on MS medium plates under LD conditions were stained with mitotracker TMRE for 5 min, followed by confocal observation.

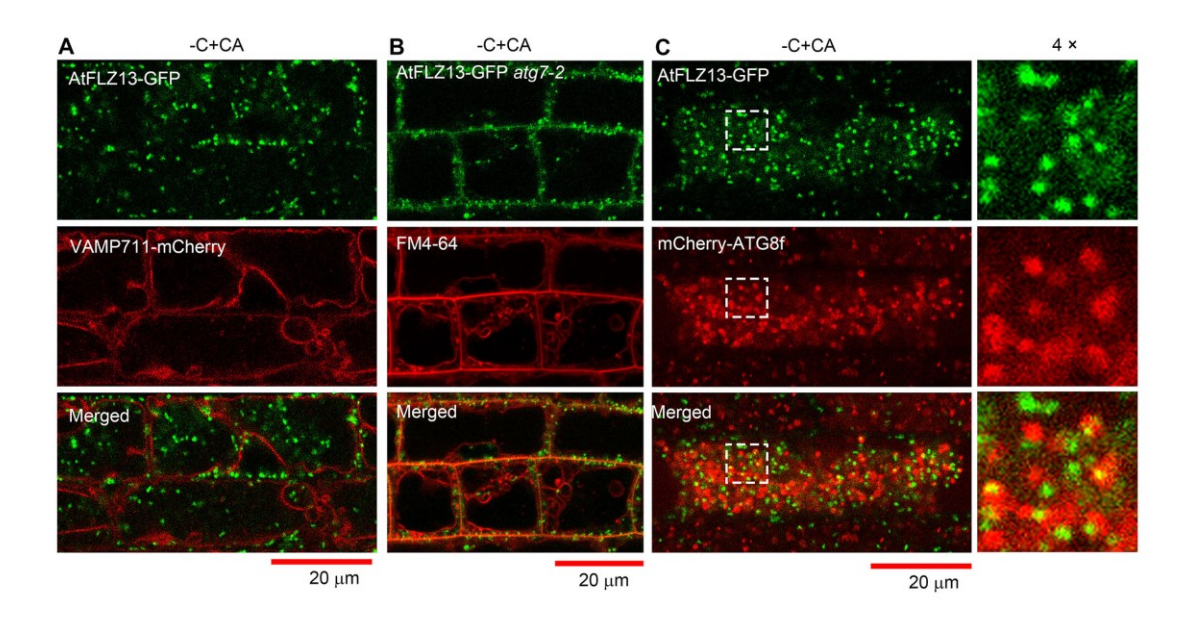


Figure S13. Subcellular localization analysis of AtFLZ13-GFP upon carbon starvation.

- (A) Confocal micrographs of Arabidopsis root cells co-expressing AtFLZ13-GFP and the tonoplast marker VAMP711-mCherry. Five-day-old seedlings grown on MS medium plates were subjected to MS-C liquid medium containing 1 Mm Conc A for 12 h before being observed.
- (B) Confocal images of AtFLZ13-GFP in *atg*7-2 root cells. Five-day-old *pUBQ10:* AtFLZ13-GFP atg7-2 seedlings grown on MS medium plates under LD conditions were subjected to MS-C liquid medium containing 5 μ M FM4-64 for 6 h, then were incubated with 1 μ M Conc A for another 12 h in darkness, followed by confocal observation.
- (C) Confocal micrographs of Arabidopsis root cells co-expressing AtFLZ13-GFP and mCherry-ATG8f (for autophagic body). Five-day-old seedlings grown on MS medium plates were subjected to MS-C liquid medium containing 1 μ M Conc A for 12 h, followed by confocal observation.

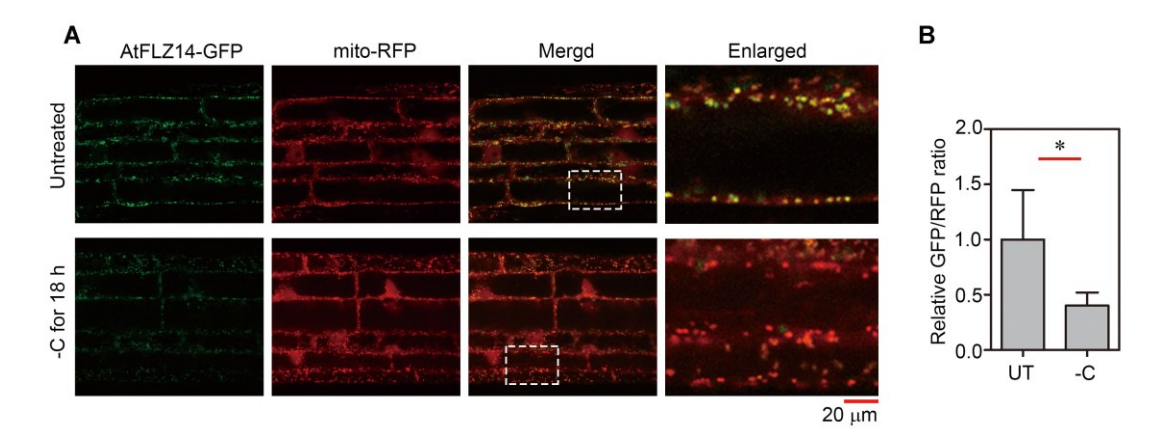


Figure S14. Subcellular localization analysis of AtFLZ14-GFP upon carbon starvation.

- (A) Confocal micrographs showing the repressive effects of carbon starvation treatments to AtFLZ14-GFP. Five-day-old seedlings grown on MS medium plates were either kept in MS medium under light or subjected to MS-C liquid medium for 18 h, followed by confocal observation. For comparison of the intensities of fluorescence, photographs of these seedlings were taken under the confocal microscope with the same parameters.
- (B) Statistic data for the relative GFP/RFP ratio. Data are means \pm SD from 7 confocal images from different roots. Statistical differences were calculated by a student's t test. The asterisk indicates statistically significant differences (*P < 0.05).

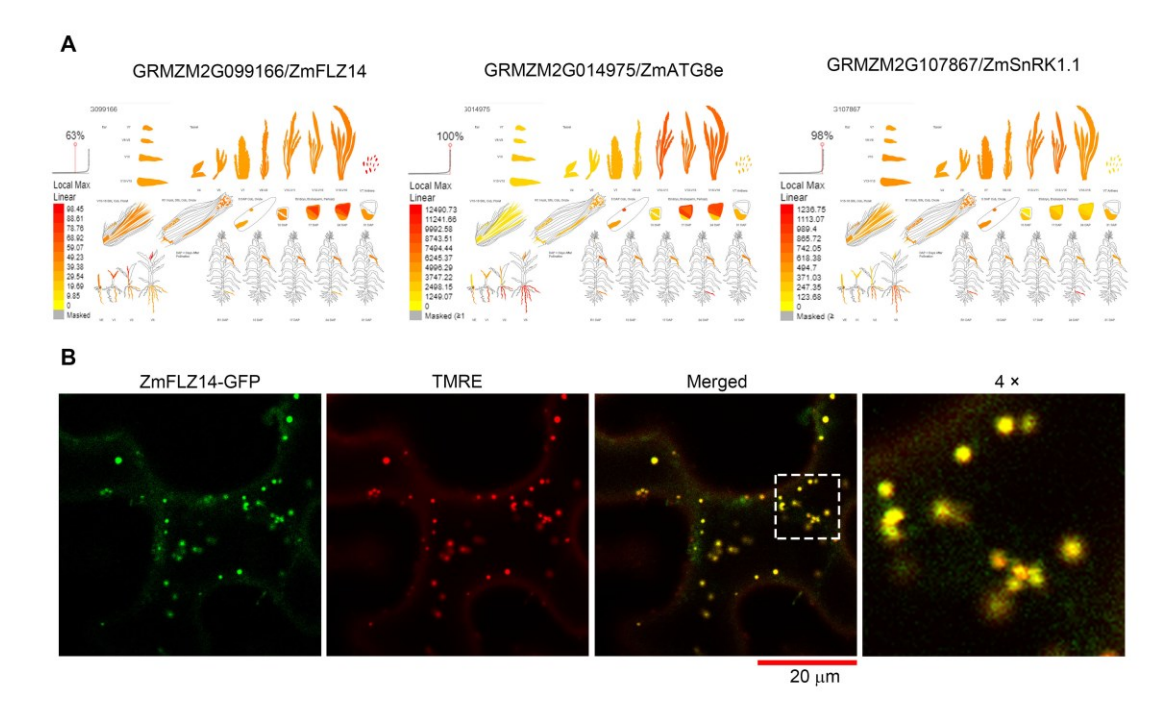


Figure S15. Expression pattern and subcellular localization of ZmFLZ14.

- (A) The expression patterns of *ZmSnRK1.1*, *ZmFLZ14* and *ZmATG8e*. The expression diagrams were generated and downloaded from the maize e-FP browser: http://bbc.botany.utoronto.ca/efp/cgi-bin/efpWeb.cgi. The color scale at the right bottom corner in each panel indicates the absolute expression levels of each individual gene: red means higher while yellow indicates lower expression levels.
- (B) Confocal micrographs of Arabidopsis leaf epidermal cells expressing a ZmFLZ14-GFP. Five-day-old *pUBQ10:ZmFLZ14-GFP* seedlings grown on MS medium plates under LD conditions were stained with mitotracker TMRE for 5 min, followed by confocal observation.